Design and Fabrication of a Photodetector array for UV/Blue Wavelength Region for Low-Light Intensity Levels Using InGaN/GaN Superlattice Structure

Dissertation submitted to
Visvesvaraya National Institute of Technology, Nagpur in partial fulfillment of the requirements for the award of the degree

Master of Technology

in

VLSI DESIGN

by

KOMMU VIJAYA RAJU

(MT23MVD013)

Under the guidance of

Dr. Nikhil Deep Gupta

Center for VLSI and Nanotechnology

Visvesvaraya National Institute of Technology Nagpur

440010 (India)

June 2025

Design and Fabrication of a Photodetector array for UV/Blue Wavelength Region for Low-Light Intensity Levels Using InGaN/GaN Superlattice Structure

Dissertation submitted to
Visvesvaraya National Institute of Technology, Nagpur in partial fulfillment of the requirements for the award of the degree

Master of Technology

in

VLSI DESIGN

by

KOMMU VIJAYA RAJU

(MT23MVD013)

Under the guidance of

Dr. Nikhil Deep Gupta

Center for VLSI and Nanotechnology

Visvesvaraya National Institute of Technology Nagpur

440010 (India)

June 2025

©Visvesvaraya National Institute of Technology, Nagpur 2023

Center for VLSI and Nanotechnology

Visvesvaraya National Institute of Technology, Nagpur

DECLARATION

I, **KOMMU VIJAYA RAJU**, hereby declare that this dissertation titled, "**Design and Fabrication of a Photodetector array for UV/Blue Wavelength Region for Low-Light Intensity Levels Using InGaN/GaN Superlattice Structure**" is carried out by me in the Department of **Center for VLSI and Nanotechnology** of Visvesvaraya National Institute of Technology, Nagpur. The work is original and has not been submitted earlier whole or in part for the award of any degree/diploma at this or any other Institution / University.

Kommu Vijaya Raju

Date:

Certificate

This to certify that the dissertation titled "**Design and Fabrication of a Photodetector array for UV/Blue Wavelength Region for Low-Light Intensity Levels Using InGaN/GaN Superlattice Structure**" is submitted by **Kommu Vijaya Raju** in partial fulfillment of the requirements for the award of the degree of **Master of Technology in VLSI Design**, VNIT Nagpur. The work is comprehensive, complete and fit for final evaluation.

Dr. Nikhil Deep Gupta
Centre for VLSI and Nanotechnology
VNIT, Nagpur.

Prof. S. B. Dhok
Head, Center for VLSI and Technology
VNIT, Nagpur
Date:

Center for VLSI and Nanotechnology

Visvesvaraya National Institute of Technology, Nagpur

June 2025

Date: _____

Non-Plagiarism Certificate

Certified that M. Tech Dissertation titled "Design and Fabrication of a Photodetector array for UV/Blue Wavelength Region for Low-Light Intensity Levels Using InGaN/GaN Superlattice Structure" submitted by Kommu Vijaya Raju (MT23MVD013) has been checked for plagiarism using TURNITIN software and the overlap is found within prescribed limits. A summary of the report is given below:

ORIGINALITY REPORT

11%	8%	7%	3%
SIMILARITY INDEX	INTERNET SOURCES	PUBLICATIONS	STUDENT PAPERS

Kommu Vijaya Raju

Date:

Dr. Nikhil Deep Gupta

Assistant Professor

Acknowledgement

I whole heartedly express my sincere gratitude to my guide, **Dr. Nikhil Deep Gupta**, Assistant Professor, Center of VLSI and Nanotechnology Department, Visvesvaraya National Institute of Technology Nagpur, Maharashtra., for giving guidance and continually providing technical assistance and good supervision during this project work.

I am profoundly grateful to **Prof. R. M. Patrikar**, **Prof. R. B. Deshmukh**, **Prof. S. B. Dhok**, **Dr. G. C. Patil**, and **Dr. Vasu Pulijala** for their unwavering support, constant encouragement, and for cultivating an academic environment at VNIT that has significantly contributed to my growth and learning. I would also like to express my heartfelt thanks to the Institute Director, Professor P. L. Patel; Dean (Academics), Professor V. R. Kalamka; and Associate Dean (Academics - PG/PhD), Professor R. V. Taiwade, VNIT Nagpur, for their steadfast support in fulfilling the academic needs of the students.

I would like to take this opportunity to thank the Indian Space Research Organization (ISRO) for providing me with the opportunity to work on the project titled, "Development of Photodetector for low intensity light levels in UV/VIS/IR wavelength regions", (grant no. YS/PD-IP/2021/333) and the Central Electronics Engineering Research Institute (CEERI) for their invaluable support and resources throughout my research.

I take this opportunity to thank all of my friends and family who have always been there for me through tough moments and counseled me on how to make the best choices. I am lucky to have a group of students from whom I have learned a great deal. I truly thank each and every one of them for their moral support and concern for me.

Kommu Vijaya Raju

ABSTRACT

Photodetectors (PDs) serve a critical role in consumer electronics to high-precision scientific and defense systems applications such as optical communication, environmental sensing, biological detection, and aerospace monitoring. However, conventional photodetector technologies, including silicon-based and arsenic-compound-based devices, face inherent challenges such as limited responsivity in the UV-blue spectrum, high exciton binding energy, and material toxicity. To overcome these limitations, this work proposes the design, simulation, and fabrication of a semipolar InGaN/GaN superlattice-based p–i–n photodetector array, epitaxially grown on a Sapphire substrate, and specifically optimized for operation in the 350–450 nm wavelength range.

The photodetector design incorporates a superlattice structure with optimized indium composition to enhance absorption and improve material quality. An array-based configuration is employed to increase the effective absorption area, thereby enhancing responsivity and enabling detection at low light intensity levels. The fabrication involves a five-step lithography process was done to fabricate the complete device including mesa etching, n-contact deposition, ITO deposition, pad opening, and final n- and p-pad metallization. The photodetector is specifically optimized for the UV-Blue spectral region (350–450 nm), where enhanced absorption due to the InGaN/GaN superlattice enables efficient detection of low-intensity light.

Four different photodetector array configurations were fabricated under this project: 2×2 series-connected array, 2×2 parallel-connected array, 3×3 array, and 4×4 array, to evaluate and compare electrical and optical performance metrics. The system is aimed at achieving high responsivity, low dark current, low noise-equivalent power (NEP), high specific detectivity, fast response time, and high quantum efficiency. Optical simulations using sentaurus are followed by full structural and electrical characterization of the devices.

The proposed design is epitaxially grown on a sapphire substrate. The layer stack comprises a GaN nucleation layer, an unintentionally doped GaN (u-GaN) buffer layer, followed by n-type GaN, a GaN/InGaN superlattice active region, p-type GaN, and a top indium tin oxide (ITO) layer that serves both as a transparent conducting contact and an anti-reflection coating.

List of figures:

Figure 1:Working of PIN photodetector [11] 4
Figure 2: Bandgap Energy with and without Bowing parameter of InGaN 9
Figure 3:CRI plot for In0.04Ga0.96N 17
Figure 4:Sentaurus workbench GUI 18
Figure 5:Photodetector showing other layers in sentaurus 24
Figure 6:Photodetector showing GaN/InGaN superlattice 24
Figure 7:Photodetector array in sentaurus 25
Figure 8:Poured acetone and IPA 26
Figure 9:Acetone Beaker and IPA Beaker placed on a heater 26
Figure 10:Scrubbed using Q-tib 27
Figure 11:Spin coated 28
Figure 12:After spin coater 28
Figure 13:Microscopic vision Surface After 1st lithography 29
Figure 14:Microscopic vision after mesa etching 31
Figure 15:Profilometer etch depth measurement 33
Figure 16:Microscopic vision I-V Characteristics Measurement to ensure etching. 34
Figure 17: I-V Characteristics 34
Figure 18:Microscopic vision after N- Contact lithography 37
Figure 19:Loading the wafer on the chamber 38
Figure 20: Remove the wafers After N-Contact deposition from the chamber. 39
Figure 21:Microscopic vision after N- Contact Deposition 40
Figure 22:Microscope image N Contact Annelling. 42
Figure 23: Microscope image after ITO lithography 44
Figure 24:Wafer's loaded on the chamber 47
Figure 25: Wafer's removed after ITO Deposition. 48
Figure 26:Microscope image after ITO Annealing. 50
Figure 27:Resistivity Measured byFour-Point Probe Method 51
Figure 28:Transmittance of reference glass wafer represents black colour 52
Figure 29:Transmittance of wafer before Annealing represents blue colour. 52
Figure 30:Transmittance of wafer After Annealing represents red colour. 53
Figure 31:Microscope image the N-type and P-type after deposition lithography. 55
Figure 32:After N and P Pad Contact Deposition removed wafer from chamber. 57
Figure 33:Microscope image after N and P Pad Contact Deposition 58
Figure 34:Microscope image after Lithography. 61
Figure 35:Microscope image of Final devices 63

Figure 36:Dicing setup 63
Figure 37:Final dicing wafer view. 65
Figure 38:Final dicing wafer view. 67
Figure 39:Transmittance of ITO vs wavelength 68
Figure 40:Optical properties (%) vs Wavelength(nm) 68
Figure 41:Probes are in contact with the n and p pad contacts 70
Figure 42:I-V characteristics of the photodetector in absence of light (-2 to 10V) 71

List of tables:

Table 1:Different bandgaps of InGaN..... 10
Table 2:CRI table for In0.04Ga0.96N..... 17
Table 3:Final specifications of the designed and fabricated device..... 22
Table 4:Optical properties(%) vs Wavelength(nm) 69
Table 5:Cut in voltages with respective different arrays..... 70
Table 6:2-D Simulation result.....70

Abbreviation:

SNR – Signal to Noise Ratio UV – Ultraviolet

PD – Photo Detector

NEP – Noise Equivalent Power

ITO – Indium Tin Oxide

CRI – Complex Refractive Index

NUV – Near-ultraviolet

Contents

1 Introduction 2

1.1 Working Principle 3

1.2 Figures of merit 4

2 MATERIAL ADVANCEMENTS AND LITERATURE REVIEW 8

2.1 Introduction 8

2.2 Group – III Nitrides 8

2.2.1 Vegard's law 8

2.3 Superlattice structure 11

2.4 Literature Review 12

2.5 Objectives 13

3 CALCULATION OF OPTICAL PROPERTIES, NUMERICAL MODELLING AND SOFTWARE FLOW 15

3.1 Complex refractive index 15

3.1.1 The Complex Refractive Index of InGaN 15

3.1.2 Real Part of the Refractive Index 15

3.1.3 Imaginary Part of the Refractive Index (Extinction Coefficient) 16

3.2 Software Flow 18

3.2.1 Synopsys Sentaurus TCAD 18

3.2.2 Ledit – Tanner EDA 18

3.3 Optical Solver 18

4 STRUCTURE DESIGN AND FABRICATION 21

4.1 Simulation 21

4.1.1 Introduction 21

4.2 FABRICATION 25

4.2.1 Cleaning process: 25
4.3 First lithography for Mesa etching 27
4.3.1 Spin Coating with Photoresist 27
4.3.2 Exposure: 28
4.3.3 Development: 29
4.3.4 Post-Baking 29
4.3.5 Procedure for Mesa Etching Using an ICP-RIE Machine 30
4.3.6 N- Contact Deposition 35
4.3.7 ITO Deposition. 42
4.3.8 Pads N type and P type Contact Deposition. 53
4.3.9 Pads opening or Deposition of Passivation layer. 59
4.3.10 Dicing for separation of each Design. 63
5 RESULTS AND DISCUSSION 67
5.1 Band diagram 67
5.2 ITO transmittance 67
5.3 Optical Properties vs Wavelength: 68
5.4 Fabricated device IV characteristics in dark 69
6 CONCLUSION AND FUTURE WORK 73
6.1 Conclusion 73
6.2 Future work 73
7 REFERENCES 74

Thesis Organization

Chapter 1:

This chapter discusses the project background and explains the working principle of the PIN photodetector.

Chapter 2:

This chapter presents a literature review of previous research on optoelectronic devices, with a particular focus on photodetectors and group III-nitride materials.

Chapter 3:

This chapter discusses the significance and calculation of the complex refractive index in determining the optical properties of group III-nitrides, numerical modelling of the software are discussed.

Chapter 4:

This chapter discusses the design of the proposed structure along with the fabrication steps involved in device development.

Chapter 5:

In this chapter, the results of the device both in simulation and fabrication are discussed.

Chapter 6:

In this chapter, the conclusion drawn from the research and future work that can be implemented to find the characteristics and further use of the device are discussed.

1

INTRODUCTION

1 Introduction

A photodetector is a device designed to sense and respond to light. It operates by absorbing incoming light energy and converting it into electrical signals, such as current or voltage. Photodetectors worked based on the photoelectric effect. The photoelectric effect means that whenever light falls on a suitable band gap semiconductor, their conductivity changes according to the photons falling on the surface.

Photodetectors serve a broad range of applications, from consumer electronics to advanced fields like space research and optical communication, with designs tailored to specific wavelengths and purposes. Among various types—MSM, Schottky, avalanche, and p-i-n. p-i-n photodiodes are favored for low-intensity light detection. Unlike MSM photodiodes, which have high speed but higher dark current and lower responsivity, p-i-n devices offer better sensitivity and lower noise. Compared to Schottky photodiodes with limited quantum efficiency, p-i-n structures benefit from a wider depletion region for enhanced absorption. Though avalanche photodiodes provide high gain, they also introduce more noise and require higher voltage. Overall, p-i-n photodiodes strike an effective balance of low noise, high responsivity, and simple operation, making them ideal for low-light applications.

The performance of a photodetector is heavily influenced by the semiconductor material employed. Although widely studied inorganic semiconductors like InGaAs, InGaSb, ZnO, GeSi, and Ga_2O_3 offer favorable properties for photodetector development, they suffer from significant limitations such as high exciton binding energy, narrow detection range, and low responsivity. Additionally, arsenic-based compounds like GaS and InGaAs require arsine (AsH_3), a highly toxic precursor, for their growth. Conventional silicon-based photodetectors, commonly used in visible light communication systems, Si based photodetectors has disadvantages due to limited wavelength range and SNR.

Group III-nitride semiconductors are widely preferred for photodetectors due to their wide bandgap, chemical and thermal stability, high breakdown field, and saturation velocity. Their cut-off wavelength can be tuned i.e., ranging from 0.7eV to 6.2eV via ternary alloying, making them ideal for harsh environments and inherently insensitive to visible and IR radiation. Recent advances in material growth and fabrication have enabled their use in a range of specialized and commercial optoelectronic devices, including photodetectors. Group III-nitride material system, the photodetector is designed using an

InGaN/GaN superlattice structure. Growth challenges due to the lack of native substrates are addressed by using sapphire with a LT-GaN nucleation layer followed by a GaN buffer layer. Considering both optical and electrical properties such as reduced lattice mismatch, lower defect density, enhanced responsivity, and improved low-light performance—the superlattice-based PIN photodetector is optimized.

In a single photodetector structure (i.e., without an array), key performance metrics such as quantum efficiency (52.19%), responsivity (0.162 A/W), and specific detectivity (5.715×10^9 Jones) demonstrated the device's potential for low-light UV-Blue detection. However, limitations such as relatively low quantum efficiency, low responsivity, a dark current of 78.38 nA, and a sensitivity of 2.06×10^3 indicated the need for further optimization. To overcome these constraints, the focus has shifted toward the development of an array-based photodetector structure. This approach offers enhanced spatial resolution, improved responsivity through signal averaging, higher quantum efficiency, better noise suppression, and superior capability in detecting weak optical signals. Therefore, array configurations are more suitable for practical applications that demand high-performance detection in the UV/Blue spectral range (350–450 nm).

1.1 Working Principle

A PIN photodetector is a semiconductor device that converts light into electrical current using a pin diode structure. The structure consists of three layers:

Ptype layer (p): Positively doped semiconductor.

Intrinsic layer (i): Undoped or very lightly doped semiconductor, which acts as the main absorption and depletion region.

Ntype layer (n): Negatively doped semiconductor.

Working Principle

Photodetectors worked based on the photoelectric effect.

1. Photon Absorption:

When incident light (photons) strikes the intrinsic region of the photodetector, photons with energy greater than or equal to the bandgap of the material are absorbed. This absorption generates electronhole pairs in the intrinsic region.

2. Carrier Separation:

A reverse bias is applied across the pin diode, creating a strong electric field in the intrinsic region The electric field quickly separates the photogenerated carriers:

Electrons move toward the n region.

Holes move toward the p region.

3. Photocurrent Generation:

The movement of electrons and holes due to the electric field constitutes a photocurrent. This current is proportional to the intensity of the incident light.

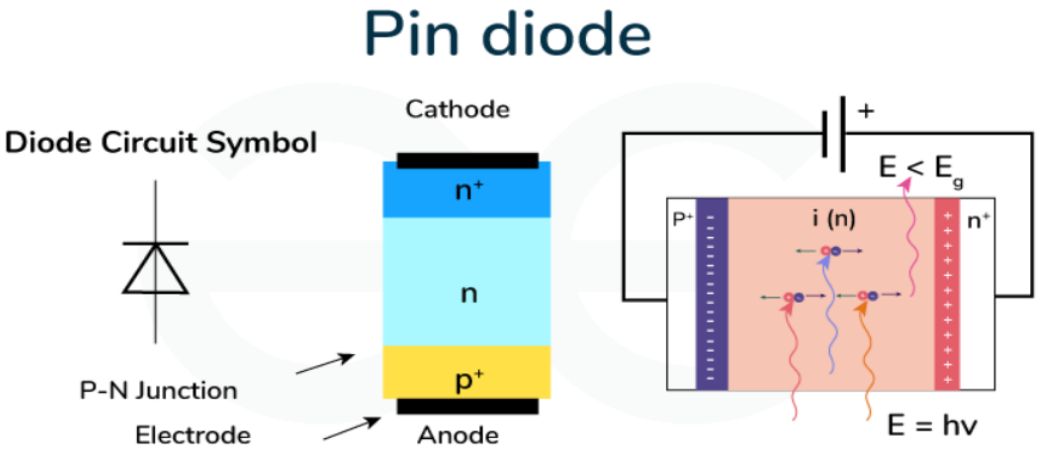

Figure 1:Working of PIN photodetector [11]

1.2 Figures of merit

The performance of a pin photodetector is evaluated based on various figures of merit, which describe its efficiency, ability to detect weak optical signals, directional response, and overall photodetection performance. These include responsivity, sensitivity, directivity, and quantum efficiency.

1. Responsivity

Measures how effectively a photodetector converts light input into electrical output. It is the ratio of output Photo current signal to incident optical power.

$$\boldsymbol{R} = \frac{\boldsymbol{I_{ph}}}{\boldsymbol{P_{opt}}} \quad \text{----------(1.1)}$$

Where, $\boldsymbol{I_{ph}}$ = Photo current

$\boldsymbol{P_{opt}}$ = Incident optical power

2. Quantum Efficiency (QE)

Describes how efficiently the detector generates charge carriers per incident photon. It is the ratio of generated electronhole pairs to the number of incident photons.

$$\eta = \frac{N_e}{N_{ph}} \quad \text{----------(1.2)}$$

Where N_e = number of electron hole pair generated

N_{ph} = Number of incident photons

3. Dark Current

Refers to the small current that flows through the detector even in the absence of light. It arises due to thermal generation of carriers.

$$I_{dark} = I_{total} \text{ (absence of light)} \quad \text{----------(1.3)}$$

4. Spectral Response

Indicates the range of wavelengths over which the photodetector is responsive or efficient.

$$SR(\lambda) = \frac{I_{ph}(\lambda)}{P_{opt(\lambda)}} \quad \text{----------(1.4)}$$

Where λ = wavelength of incident light

5. Response Time

The time the detector takes to respond to incoming light. It defines how fast the photodetector can react to changes in light intensity.

$$\tau = \frac{1}{2\pi f_c} \quad \text{----------(1.5)}$$

6. Gain

The ratio of the output photocurrent to the initial photocurrent generated by absorbed photons. Some photodetectors have internal mechanisms to amplify the signal.

$$G = \frac{I_{out}}{I_{photogenerated}} \quad \text{----------(1.6)}$$

7. Noise Equivalent Power (NEP)

Represents the amount of incident light power needed to generate a signal equal to the noise level. Lower NEP indicates higher sensitivity.

$$NEP = \frac{I_n}{R} \quad \text{---------- (1.7)}$$

Where I_n = noise current (A/$\sqrt{Hz}$)

R = responsivity (A/W)

8. Frequency Bandwidth

The range of signal frequencies the detector can handle effectively. Typically defined at

the 3 dB point, where the responsivity drops to 70.7% of its peak.

$$\mathbf{BW = f_{3dB}} \quad \text{----------(1.8)}$$

9. Detectivity (D)

The inverse of NEP, indicating how well a detector can distinguish weak signals from noise. Higher detectivity means better performance in lowlight conditions

$$D^* = \frac{\sqrt{A \cdot \Delta f}}{NEP} \quad \text{----------(1.9)}$$

Where A = detector area (cm^2)

$\boldsymbol{\Delta f}$ = bandwidth (Hz)

2

MATERIAL ADVANCEMENTS AND LITERATURE REVIEW

2 MATERIAL ADVANCEMENTS AND LITERATURE REVIEW

2.1 Introduction

The previous chapter introduced the fundamentals of photodetectors, including their operational principles, key performance metrics (figures of merit), and outlined the central problem motivating this research. Building upon that foundation, this chapter focuses on the selection and justification of the materials used in the proposed photodetector design.

Group III-nitride semiconductors, particularly InN, GaN, and AlN, offer a compelling material platform for optoelectronic devices due to their wide and tunable bandgap range. The bandgap can be engineered from 0.7 eV (InN) through 3.42 eV (GaN) up to 6.2 eV (AlN), thereby covering a broad spectral range from the ultraviolet (UV) to the infrared. This tunability makes them exceptionally suitable for wavelength-specific detection, particularly in the UV/blue region.

Taking these properties into account, the InGaN/GaN material system emerges as a particularly advantageous choice for the design of a photodetector targeting the UV to blue wavelength spectrum, especially under low-light intensity conditions. By adjusting the indium content in the InGaN alloy, the bandgap of the active region can be finely tuned to achieve peak responsivity at desired UV/blue wavelengths. Thus, the present study utilizes a superlattice structure combining InGaN and GaN to serve as the active absorption region within a p-i-n photodiode configuration, optimizing both spectral sensitivity and quantum efficiency.

2.2 Group – III Nitrides

2.2.1 Vegard's law

In semiconductor materials like $In_xGa_{1-x}N$, tuning the indium content (denoted by the mole fraction x) allows precise control over both the bandgap energy and, consequently, the cutoff wavelength of the material. This is especially useful for optoelectronic applications such as light emitting diodes (LEDs), laser diodes, and photodetectors, where the device performance is highly sensitive to the bandgap of the active region material.

$In_xGa_{1-x}N$ is a ternary alloy formed by combining InN and GaN, both of which are direct bandgap semiconductors with different lattice constants and bandgap energies:

Bandgap of GaN (x = 0): 3.42 eV

Bandgap of InN (x = 1): 0.7 eV

To estimate the bandgap of $In_xGa_{1-x}N$ at intermediate compositions, Vegard's law is used. For a simple linear interpolation:

$E_{g,InxGa(1-x)N} = x.E_{g,InN}+(1-x).E_{g,GaN}$ ----------(2.1)[1]

However, due to the nonlinear behavior of the bandgap in mixed semiconductors, a bowing parameter (b) is introduced to improve accuracy:

$E_{g,InxGa(1-x)N} = x.E_{g,InN} + (1-x).E_{g,GaN} - bx(1-x)$ ----------(2.2) [1]

Where:

$E_{g,InN} = 0.7eV$

$E_{g,GaN} = 3.42\ eV$

b = 1.43 eV (bowing parameter)

The cutoff wavelength (λ_s) corresponding to the bandgap energy is given by the relation:

$\lambda_c = \frac{hc}{Eg}\frac{1240}{Eg}$ (Eg in eV, λc in nm) ----------(2.3)

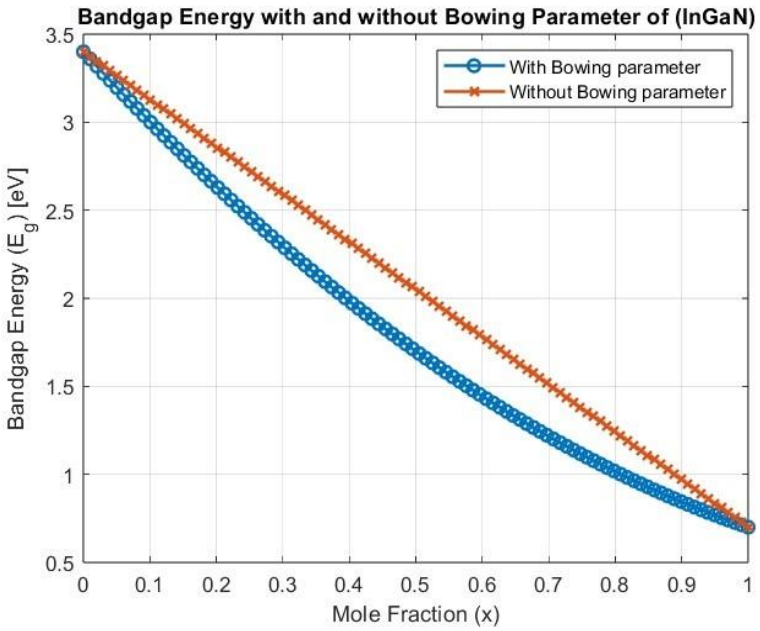

Figure 2: Bandgap Energy with and without Bowing parameter of InGaN

Observations:

1. Xaxis (Mole Fraction x): Represents the indium content in $In_xGa_{1-x}N$, ranging from 0 (pure GaN) to 1 (pure InN).
2. Yaxis (Bandgap Energy E_g [eV]):Denotes the bandgap energy of the material in electron volts (eV), ranging approximately from 0.7 eV (InN) to 3.42 eV (GaN).
3. Blue Curve (With Bowing Parameter): Shows the nonlinear variation of bandgap energy with composition when including the bowing parameter (b = 1.43 eV) in Equation 2.2:
4. Orange Curve (Without Bowing Parameter): Depicts a linear interpolation of the bandgap as per Vegard's law (Equation 2.1), ignoring the curvature:
5. NonLinearity of Bandgap Variation:The blue curve clearly deviates downward from the orange line,especially in the midcomposition range (x = 0.3–0.7). This indicates that the bandgap does not decrease linearly with increasing In composition.The bowing parameter

captures the nonlinear interaction between GaN and InN atoms in the alloy, such as differences in electronegativity, lattice mismatch, and strain effects.

6. Importance of the Bowing Effect: Ignoring the bowing parameter would result in overestimating the bandgap for a given composition, leading to inaccurate predictions of device behavior. For example, at x = 0.5, the bandgap with bowing is much lower than predicted by linear interpolation—this has significant implications for the design of photodetectors and LEDs.
7. Material Selection and Design Implications: For UV detectors, precise control of the bandgap is critical to tune the cutoff wavelength. As mentioned earlier, for detecting light at 380 nm, an $In_{0.04}Ga_{0.96}N$ composition (x = 0.04) is suitable. This corresponds to a bandgap of ~3.26 eV, which is accurately represented only when the bowing parameter is considered.
8. Scientific Justification: The diagram provides visual evidence supporting the need to use in simulations and modeling of InGaNbased devices.It validates the decision to use a 4% indium composition, which not only matches the required optical characteristics but also maintains high material quality due to minimal strain.

Table 1:Different bandgaps of InGaN

Mole Fraction (x)	**Material ($In_xGa_{(1-x)}N$)**	**Energy Bandgap (eV)**
0	GaN	3.42
0.04	$In_{0.04}Ga_{0.9}N$	3.256
0.05	$In_{0.05}Ga_{0.95}N$	3.21607
0.1	$In_{0.1}Ga_{0.9}N$	3.0193
0.2	$In_{0.2}Ga_{0.8}N$	2.6472
0.4	$In_{0.4}Ga_{0.6}N$	1.9888
0.6	$In_{0.6}Ga_{0.4}N$	1.4448
0.8	$In_{0.8}Ga_{0.2}N$	1.1052
1	InN	0.7

From the table and calculations:

At x = 0.04 (4% In):

$$E_g = 3.256 \text{ eV} \Rightarrow \lambda c = \frac{1240}{3.256} \approx 380.7 \text{ nm}$$

why i am prefferring 4% of indium composition because:

This wavelength lies within the near-ultraviolet (NUV) range, very close to 380 nm, which is

commonly targeted in UV photodetection applications.

A. Material Quality and Growth Considerations:

   Lower In composition (e.g., 4%) is easier to grow using metalorganic chemical vapor deposition (MOCVD) or molecular beam epitaxy (MBE) on GaN substrates.

   High In content leads to lattice mismatch with GaN, resulting in defects and degradation of crystal quality. At 4% In, the strain and defect density are minimal, ensuring high material quality and device reliability.

B. Sharp Bandgap Control with Minimal Bowing Effect:

   At low x values, the bowing effect is less pronounced, and linear interpolation is often sufficient. This simplifies modeling and reduces uncertainty.

C. Suitability for pin Photodetector:

   A pin structure with $In_{0.04}Ga_{0.96}N$ in the intrinsic region combines efficient absorption at 380 nm with good carrier mobility and low defect density, crucial for fast response and high sensitivity.

For our photodetector, photocurrent can be increased and the dark current can be decreased by reducing the probability of recombination of photogenerated electrons and holes, and this can be achieved by fabricating high-quality and defect-free devices, using heterojunctions with type-II band alignment i.e., InGaN/GaN superlattice is formed using staggered gap which result into the effective separation of charge carriers.

2.3 Superlattice structure

Design Considerations of InGaN/GaN SuperlatticeBased Photodetector

In the development of highperformance photodetectors, quantum efficiency is a critical parameter that is strongly influenced by the optical absorption characteristics and thickness of the active layer. A thicker absorption layer generally enhances the quantum efficiency by capturing more incident photons. However, this increased thickness leads to a tradeoff, particularly in reducing the bandwidth and limiting the speed of the photodetector due to longer carrier transit times.

To address this challenge, a superlattice structure composed of alternating thin layers of InGaN and GaN is utilized in place of a conventional bulk or thick singlelayer active region. The InGaN/GaN superlattice structure, incorporated into the intrinsic (i) region of a pin photodetector, offers a refined mechanism for carrier generation and collection. Due to the reduced thickness of individual layers and the engineered band alignment, this structure promotes quantum tunneling of carriers. The proximity of adjacent potential wells allows the wavefunctions of charge carriers to overlap, enhancing tunneling probability and facilitating efficient carrier transport across the structure.

This approach is contrasted with multiple quantum well (MQW) structures, where the wider

barriers between wells significantly reduce tunneling. In MQW configurations, carriers are typically confined within wells, and the probability of interwell tunneling is minimal unless specific electric field conditions are met. Consequently, MQWs tend to trap carriers, leading to reduced extraction efficiency.

In contrast, the superlattice design, by ensuring thinner barriers, enables continuous movement of carriers, thereby improving both the collection efficiency and overall response speed of the device. This balance of optical absorption and highspeed operation makes the InGaN/GaN superlattice structure a compelling choice for photodetectors requiring both sensitivity and fast response. Hence, the use of a superlattice in the intrinsic region of a pin photodetector aligns well with the design goals of high quantum efficiency and highspeed performance, as necessitated by modern optoelectronic applications.

2.4 Literature Review

1. "InGaN/GaN Superlattice UV PD under Low Light" addressed the low-light intensity regime by fabricating an InGaN/GaN superlattice-based p-i-n photodetector designed for UV/blue detection. Their structure incorporated a 50-period SL absorber, optimized for 385 nm detection. At a light intensity of 1 μW/cm², the device achieved an external quantum efficiency of 52.19%, with photocurrent reaching 161.74 nA and dark current as low as 78 pA. Simulation using Sentaurus TCAD confirmed high absorption and minimal reflection in the 370–400 nm range. The structure also utilized an ITO transparent contact that served dual roles as anti-reflection coating (ARC) and electrical contact. Performance validated by TCAD simulation and real measurements.
2. "GaN Homojunction pin UV Photodetectors" This foundational study focused on GaNbased homojunction pin photodetectors grown by MOCVD. Devices demonstrated low dark current density (~2 nA/cm² at −10 V) and an external quantum efficiency (EQE) of ~45% at 362 nm. However, an optical "dead zone" in the pGaN layer limited full photon conversion. Their driftdiffusion model helped identify how surface recombination and electron diffusion length influence EQE, setting performance benchmarks for GaN PDs.
3. "GaN pin PDs on Patterned Sapphire Substrates" This work showcased the advantages of patterned sapphire substrates (PSS) in improving crystalline quality. GaN pin photodetectors on PSS showed as Reduced dislocation density (~6–8 × 10^7 cm^{-2}), Low dark current (~5.1 nA/cm²), High UV/visible rejection ratio (>10^4), Peak external quantum efficiency(EQE) of ~65% at 360 nm.The study demonstrated how substrate engineering can significantly enhance PD performance for UV detection.
4. "Simulation of InGaN/GaN pin Photodiodes" Using SILVACO–Atlas, a photodiode with

a 0.1 μm intrinsic $In_{0.1}Ga_{0.9}N$ layer was modeled. Results showed as Peak responsivity of 0.244 A/W at 384 nm, Breakdown voltage up to 38 V, Cutoff frequency up to 4 GHz (at 1.5 μm ilayer). This study validated simulation as a powerful tool to optimize InGaN/GaN pin structures before fabrication, especially for UV/blue range detection.

5. "InGaN/GaN Heterojunction Phototransistors" A highspeed phototransistor using a 15period $In_{0.15}$GaN(4nm)/GaN(1.8nm) superlattice with a dopantfree polarizationinduced base was fabricated. Key outcomes are Responsivity up to 470 A/W at 402 nm, Response time of \~3.4 ns, Biastunable spectral response (narrowband at low bias, broadband at high bias). Though focused on visible light, this work demonstrated the potential of superlattice structures in enhancing responsivity and spectral control without filters.
6. "Indium Composition in InGaN/GaN MQWs" This study analyzed InGaN/GaN multiple quantum well (MQW) solar cells with different indium contents. Findings included Optimal performance below 20% indium composition, At 28% indium, dislocations increased significantly, degrading performance.This insight is critical for PD design excessive indium in superlattices can introduce defects that reduce carrier lifetime and detection sensitivity.

2.5 Objectives

The primary objective of this research is the design, fabrication, and characterization of a GaNbased photodetector array capable of operating under low light intensity conditions, specifically targeting the ultraviolet (UV) to blue wavelength regions. The motivation stems from the need to enhance the performance metrics—figures of merit—of current photodetector technologies, aiming to surpass those reported in existing literature.

By utilizing a photodetector array instead of a single device, the proposed design capitalizes on the increased optical absorption area, which directly contributes to improved detection capabilities. Key performance improvements targeted in this work include the reduction of dark current, enhancement of responsivity, increased quantum efficiency, and overall improvement in device reliability. These enhancements are crucial for enabling more sensitive and efficient photodetection in lowlight environments.

The research methodology encompasses the full cycle of device development: design optimization through simulation, fabrication using advanced semiconductor processing techniques, and experimental characterization of the fabricated devices. The ultimate goal is to develop a highperformance, reliable photodetector array that can serve a wide range of applications in fields requiring UV to blue light detection, including environmental monitoring, biomedical sensing, flame detection, and optical communication systems.

3

CALCULATION OF OPTICAL PROPERTIES, NUMERICAL MODELLING AND SOFTWARE FLOW

3 CALCULATION OF OPTICAL PROPERTIES, NUMERICAL MODELLING AND SOFTWARE FLOW

3.1 Complex refractive index

To perform the numerical simulation first of all we need to calculate the material properties of materials which we used for design. in that two material properties are considerable i.e. Energy gap and CRI.

3.1.1 The Complex Refractive Index of InGaN

The optical properties of semiconductors, particularly their interaction with light, are primarily governed by the refractive index. The refractive index defines the speed at which light propagates through a material relative to the speed of light in a vacuum. When light encounters a medium, it interacts with the electronic structure of the material, altering the material's dielectric response. This results in a complex dielectric constant, which in turn defines the complex refractive index of the material.

The complex refractive index N(\lambda) is given by:

$$N(\lambda) = n(\lambda) + i\,k(\lambda)$$

where:

$n(\lambda)$: real part representing the phase velocity of light in the material,

$k(\lambda)$: imaginary part known as the extinction coefficient, which accounts for the energy loss due to absorption,

λ: wavelength of the incident light.

The presence of the imaginary component leads to attenuation of the electromagnetic wave as it propagates through the material. This attenuation is exponential and is characterized by the absorption coefficient alpha, which determines how rapidly light intensity decays inside the material. A higher n value slows light down more, while a smaller k indicates a more optically transparent material.

3.1.2 Real Part of the Refractive Index

The real part of the refractive index is computed using an empirical relationship derived for InGaN alloys, based on the photon energy E_{ph} and the bandgap E_g of the material:

$$n = \sqrt{A\left[\frac{E_{ph}}{E_g}\right]^{-2}\left[2 - \sqrt{1+\left[\frac{E_{ph}}{E_g}\right]} - \sqrt{1-\left[\frac{E_{ph}}{E_g}\right]}\right] + B} \quad \text{----------(3.1)[1]}$$

Where:

A and B are materialdependent coefficients, calculated as functions of the indium composition x in $In_xGa_{1-x}N$:

$A(ln_xGa_{(1-x)}N) = 13.55x + 9.31(1- x)$ ----------(3.2) [1]

$B(ln_xGa_{(1-x)}N) = 2.05x + 3.03(1 -x)$ ----------(3.3) [1]

These expressions ensure that the refractive index changes smoothly with the alloy composition, providing wavelength and compositiondependent modeling. It is Represented by the red solid curve.It shows the material's ability to bend or refract light as it passes through. At shorter wavelengths (around 0.2 to 0.4 μm), the refractive index is high, peaking around 2.9. It decreases gradually as the wavelength increases, stabilizing around 2.4 for wavelengths greater than 0.8 μm. This indicates the dispersion of light, where the refractive index decreases as wavelength increases (normal dispersion).

3.1.3 Imaginary Part of the Refractive Index (Extinction Coefficient)

The imaginary part k is directly related to the absorption coefficient \alpha by the equation:

$k = \frac{\lambda\alpha}{4\pi}$

The absorption coefficient \alpha, representing how strongly the material absorbs light at a given wavelength, is defined empirically for InGaN as:

$\alpha(ln_xGa_{(1-x)}N) = \sqrt{C[E_{ph} - E_g] + D[E_{ph} - E_g]^{-2}}$ ----------(3.4)[1]

Where C and D are fitting parameters that also vary with indium composition:

$C(x) = 3.525 - 18.29x + 40.22x^2 - 37.52x^3 + 12.77x^4$ -------(3.5)[1]

$D(x) = 0.665 + 3.616x - 2.460x^2$ ----------(3.6)[1]

An alternative simplified expression used in some modeling contexts is:

$\alpha(ln_xGa_{(1-x)}N) = 2.2 \times 10^5 \sqrt{\left[\frac{1.24}{\lambda}\right] - E_g}$ ----------(3.7)[1]

These equations allow for the wavelengthdependent modeling of optical absorption in InGaN, making them highly useful for simulating the device's optical response.Extinction Coefficient is Represented by the blue dashed curve. It indicates the material's absorption of light, with higher values representing stronger absorption. The extinction coefficient is significant at shorter wavelengths (peaking around 0.4 μm) and then rapidly decreases, becoming negligible at wavelengths beyond ~0.8 μm. This suggests that the material is more absorptive in the UV visible range and relatively transparent in the near-infrared range.

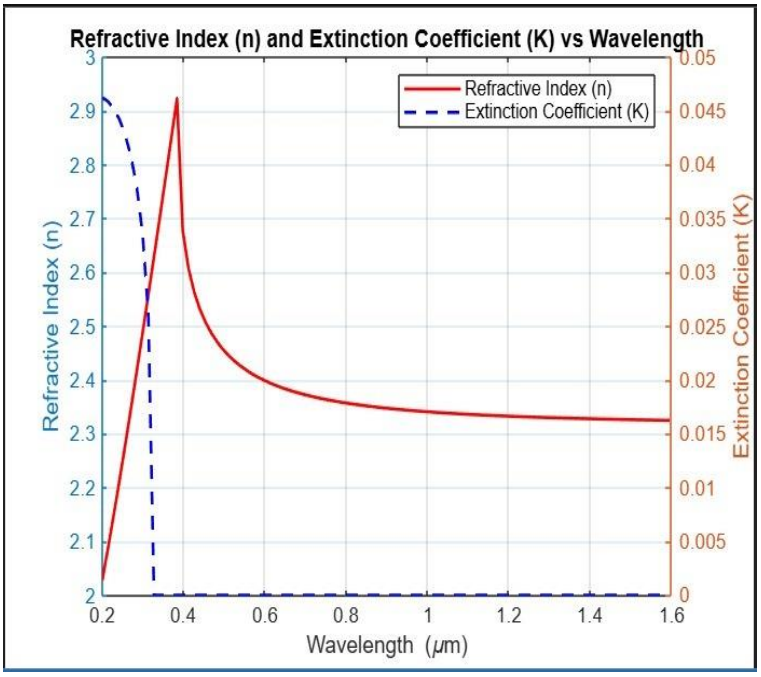

Figure 3:CRI plot for In0.04Ga0.96N

This plot illustrates the variation of the refractive index (n) and the extinction coefficient (k) of a material as a function of wavelength in the spectrum from 0.2 μm to 1.6 μm. These optical properties are critical for understanding the interaction of light with the material. Material Behavior in Different Wavelengths i.e In the UV-visible region (0.2–0.4 μm): The high refractive index and extinction coefficient imply strong light interaction, including significant refraction and absorption.In the infrared region (beyond ~0.8 μm): The material exhibits low absorption (low k) and a nearly constant refractive index (n), making it suitable for applications requiring transparency in this region.

Table 2:CRI table for In0.04Ga0.96N

Wavelength (μm)	**n**	**k**
0.35	2.2415837	0.2475373
0.355	2.3123816	0.2297071
0.36	2.3878183	0.2092498
0.365	2.4693713	0.1852974
0.37	2.5597889	0.1562508
0.375	2.6654608	0.1184189
0.38	2.8135247	0.0562254
0.385	2.783629	0
0.39	2.7209412	0
0.395	2.6805144	0
0.4	2.6501205	0
0.405	2.6256904	0
0.41	2.6052819	0
0.415	2.5877938	0
0.42	2.5725331	0

3.2 Software Flow

3.2.1 Synopsys Sentaurus TCAD

The entire simulations are done using Synopsys Sentaurus TCAD workbench. Sentaurus workbench allows us to create, modify and manage the process flows. Here the structure of our design is made using SDE (Sentaurus Structure Editor) which is added to the workbench. Then sdevice tool is also added to the gui, which is used for the calculation of optical generation in the structure created in sde.

Svisual is a tool used for examining both the structures and the simulations done on the workbench gui using sde and sdevice After all the simulations are completed, we can observe the structure created and also the plot of optical generation of the active region.

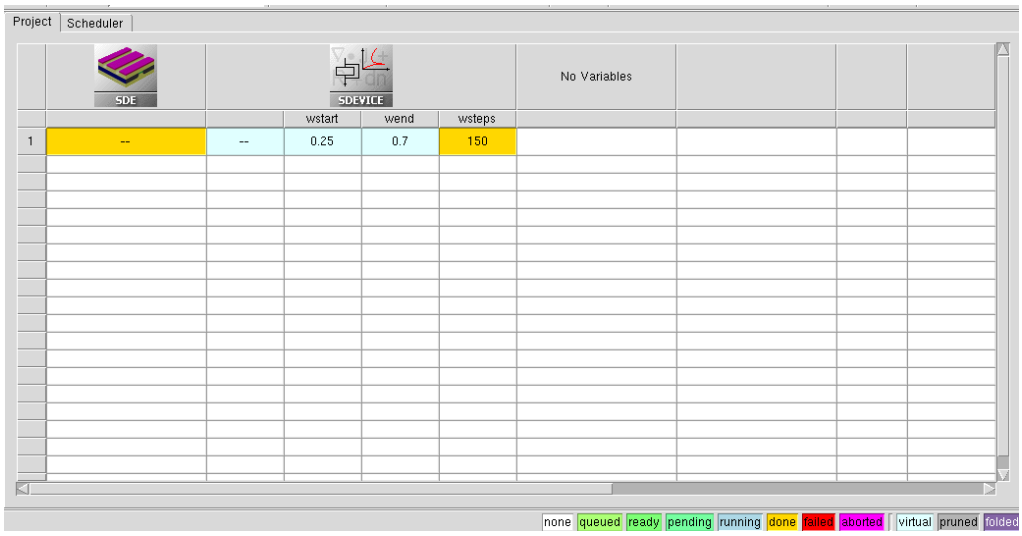

Figure 4:Sentaurus workbench GUI

3.2.2 Ledit – Tanner EDA

Ledit is a Tanner EDA tool used to create layouts and masks for the fabrication of the semiconductor devices. We have designed the mask for the UV photodetector array using this tool. We need five levels of lithography for the fabrication of our device. All the five levels are created on a single tool and adjusted geometrically so that a single mask can be used for all the lithography steps.

3.3 Optical Solver

There are many types of optical solvers in the sdevice of Sentaurus TCAD to compute optical generation, and other optical properties. The optimal combination of result, accuracy and computation time is used to choose a specific technique. In this investigation, the optical solver called EMW or SDEVICE Tool is used for our device simulations based on multiple factors.

In optics, to calculate the propagation of plane waves through medium containing multiple layers, the transfer-matrix method is used. When a plane wave encounters a layered material, it is reflected and transmitted at the layer boundaries. These reflections generate their own reflections and transmissions continuously. Fresnel equations are used to compute the intricate magnitude of these transmitted and reflected waves, and these equations are then made simpler utilizing matrix methods.

4

STRUCTURE DESIGN AND FABRICATION

4 STRUCTURE DESIGN AND FABRICATION

4.1 Simulation

4.1.1 Introduction

The design and optimization of photodetector arrays demand the fulfillment of several key performance metrics: high visible light rejection, high responsivity, enhanced quantum efficiency at the target wavelength, low dark current, linear response to incident optical power, and rapid temporal response. These characteristics are essential for reliable operation in advanced optoelectronic and imaging systems.

A fundamental challenge in achieving high quantum efficiency lies in the inherent tradeoff between absorption and carrier transport properties of the active region. While increasing the thickness of the absorption layer can improve photon absorption and thus quantum efficiency, it concurrently introduces longer carrier transit times. This results in reduced bandwidth and slower device response.

To overcome this limitation, the proposed device employs a carefully engineered superlattice structure composed of alternating thin layers of InGaN and GaN within the intrinsic region of a pin photodetector. This InGaN/GaN superlattice enhances quantum tunneling and carrier transport through wavefunction overlap between adjacent quantum wells. Compared to conventional thicklayer designs, the superlattice offers improved charge carrier collection efficiency, lower transit time, and higher speed without sacrificing optical absorption.

The complete layer structure of the proposed photodetector is meticulously designed as follows:

Sapphire substrate: Provides mechanical support and optical transparency in the UVvisible range.Lowtemperature GaN (LTGaN): Serves as a nucleation layer to promote highquality GaN epitaxial growth. Undoped GaN buffer layer: Reduces lattice mismatch between the substrate and the ntype GaN layer. Sidoped GaN: Functions as the ntype region, facilitating efficient electron transport.InGaN/GaN superlattice: Acts as the intrinsic (i) region, enabling enhanced photon absorption and carrier transport. Mgdoped GaN: Serves as the ptype layer, forming the pin junction necessary for carrier separation under illumination.Indium Tin Oxide (ITO): A transparent conductive layer deposited on the surface to minimize optical reflection losses and provide optical confinement in the active region.

This carefully engineered layer stack not only addresses the optical and electrical performance constraints but also ensures improved device parameters such as high responsivity, low dark current, reduced noise equivalent power (NEP), elevated specific detectivity (D), fast response time, and high sensitivity. The incorporation of the superlattice structure proves vital in striking a balance between

efficient light absorption and rapid carrier extraction, thus enabling the realization of a highperformance photodetector suitable for advanced photonic applications.

Table 3:Final specifications of the designed and fabricated device

SPECIFICATION	**VALUE**
Thickness of Sapphire substrate (Al_2O_3)	450 µm
Thickness of LT-GaN	30 nm
Thickness of undoped GaN	1 µm
Thickness of n-GaN	2 µm
Magnesium doping concentration of p-GaN	$3 \times 10^{19}/cm^3$
Thickness of Superlattice (InGaN/GaN)	1nm each of 50
Thickness of p-GaN	250nm
Thickness of ITO	180nm
Silicon doping concentration of n-GaN	$5 \times 10^{18}/cm^3$
Metal for n contact (Ti/Al/Ni/Au)	30/100/20/100 nm
Metal for pad contacts (Ti/Au)	20/50 nm
Thickness of Superlattice (InGaN/GaN)	1nm each of 50
Area of pad contacts for both p- and n-contacts	100 µm × 100 µm
Diameter of each circular active region (photodetector)	100 µm
Center-to-center horizontal spacing between photodetectors	140 µm
Center-to-center vertical spacing between photodetectors	120 µm
Horizontal spacing between adjacent detectors	40 µm
Vertical spacing between adjacent detectors	20 µm

The proposed device structure has been meticulously designed to achieve optimal optoelectronic performance parameters by leveraging the benefits of group III nitride semiconductor materials and superlattice engineering.

The layer stack begins with a Sapphire (Al_2O_3) substrate, chosen for its excellent optical transparency

in the UVvisible range and mechanical stability. A 30 nm lowtemperature GaN (LTGaN) layer is grown atop the substrate to act as a nucleation layer, promoting highquality epitaxial growth of subsequent GaN layers. This is followed by a 1 μm undoped GaN buffer layer, which plays a critical role in mitigating the lattice mismatch between the sapphire substrate and the doped GaN layers, thereby reducing defect densities.

The ntype region comprises a 2 μm thick silicondoped GaN layer with a doping concentration of 5×10^{18} cm^{-3}. This ensures efficient electron transport and electrical conductivity. The intrinsic region, which is central to photon absorption and carrier generation, is realized using a superlattice structure composed of 50 alternating layers of 1 nm InGaN and 1 nm GaN. The superlattice configuration enhances photon absorption at the targeted UV wavelength (380 nm) and facilitates rapid carrier transport via quantum tunneling mechanisms, which is not achievable in bulk or thick singlelayer active regions.

The ptype region is formed using a 250 nm thick Mgdoped GaN layer with a doping concentration of 3×10^{19} cm^{-3}. This facilitates efficient hole transport and ensures the formation of a welldefined pin junction for effective carrier separation under illumination. To reduce surface reflectance and enable better optical confinement, a 180 nm thick Indium Tin Oxide (ITO) layer is deposited on top of the structure, which also serves as a transparent conductive electrode.

Electrical contacts are formed using a Ti/Al/Ni/Au metal stack (30/100/20/100 nm) for the ncontact and a Ti/Au (20/50 nm) stack for the pad contacts. Both p and n pad contacts are patterned with an area of 100 μm × 100 μm, and the radius of the active region is maintained at 100 μm to ensure uniform light absorption and current collection.

To detect a peak wavelength of 380 nm (equivalent to a photon energy of 3.26 eV), the InGaN layer is precisely engineered with an indium composition of approximately 4%. This corresponds to a bandgap of about 3.255 eV, derived using Vegard's law, which also supports lattice matching for epitaxial growth on GaN layers.

The entire device was modeled and simulated using the Synopsys Sentaurus TCAD suite. The structural design was created using Sentaurus Structure Editor, and the optical generation profile was computed using the Transfer Matrix Method (TMM) within the sdevice tool in Sentaurus Workbench. This simulation workflow enables precise modeling of optical absorption and carrier dynamics within

the superlattice region.

The resulting design is expected to exhibit a range of favorable characteristics, including: High responsivity in the UV region, Enhanced quantum efficiency, Low dark current and noise equivalent power (NEP), High specific detectivity (D),Fast response time, High sensitivity and linearity with respect to incident optical power.

These features make the proposed InGaN/GaN superlatticebased photodetector an excellent candidate for nextgeneration UV photodetection applications, particularly in areas requiring highspeed and lownoise performance.

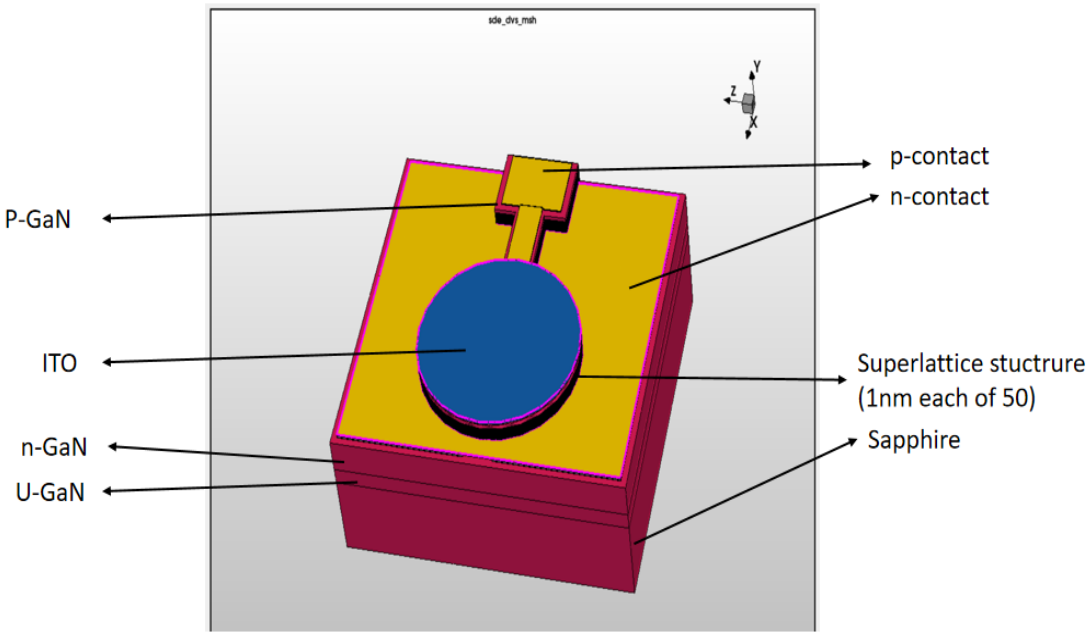

Figure 5:Photodetector showing other layers in sentaurus

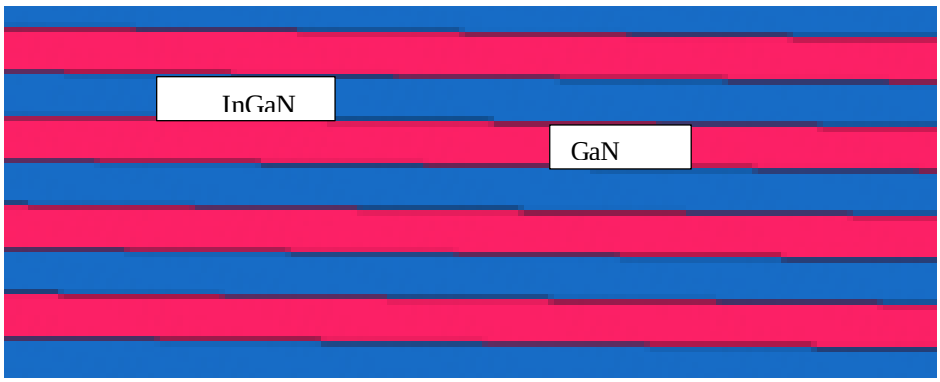

Figure 6:Photodetector showing GaN/InGaN superlattice

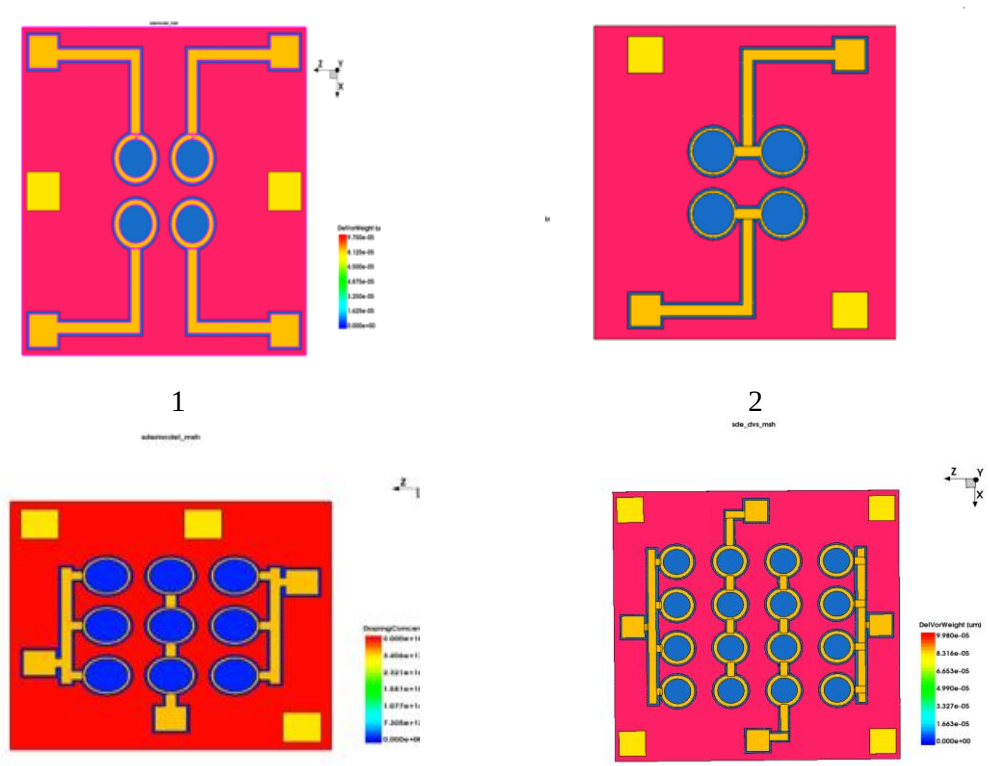

1 2

3 4

Figure 7:Photodetector array in sentaurus

4.2 FABRICATION

4.2.1 Cleaning process:

1. Beakers were cleaned using chromic acid and thoroughly dried.
2. Three beakers were prepared, each filled with acetone, IPA, and DI water, respectively.

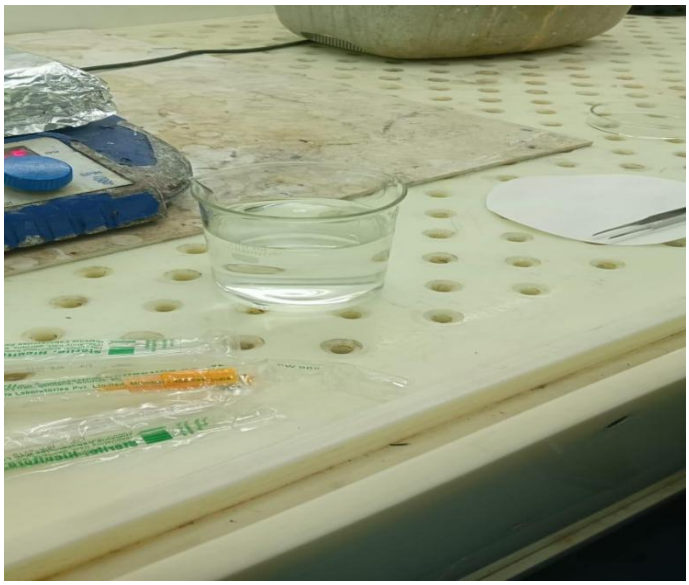

Figure 8:Poured acetone and IPA

3. The beakers containing acetone and IPA solutions were placed on a heater set to 160℃.

Figure 9:Acetone Beaker and IPA Beaker placed on a heater

4. The wafer was placed in a boat and immersed in the acetone solution to remove organic impurities.
5. After 15 minutes, the boat was removed from the acetone solution.
6. The boat was then dipped into the DI water to eliminate any remaining impurities on the wafer.
7. Subsequently, the stand was immersed in the IPA solution to remove residual impurities and any remaining acetone on the wafer. After 10 minutes, the stand was removed from the IPA solution.

8. The wafer surface was scrubbed using Q-tib during rinsing for additional cleaning.

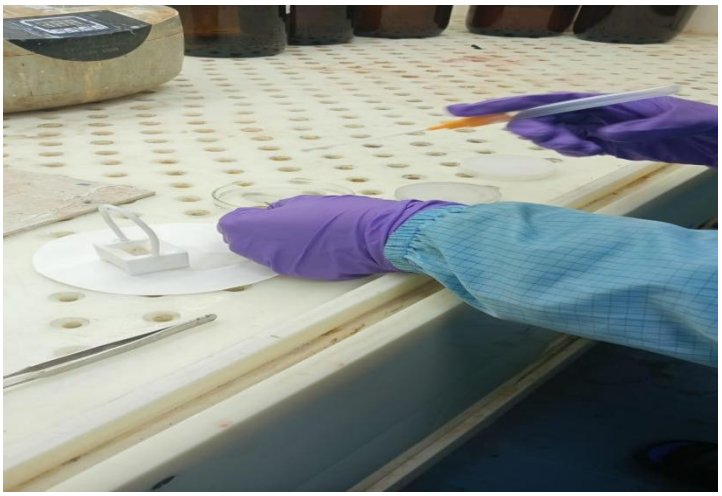

Figure 10:Scrubbed using Q-tib

9. Finally, nitrogen gas was used to dry the wafer, completing the process and making it ready for use.

4.3 First lithography for Mesa etching

4.3.1 Spin Coating with Photoresist

Step 1: Initial Coating

The S1818 photoresist was applied to the sapphire epitaxy wafer.

The wafer was spin-coated initially at 1000 rpm for 30 seconds with an acceleration rate of 200 rpm/s to ensure an even spread of the photoresist across the surface.

Following this, the wafer was baked at 120℃ for 15 minutes to enhance the adhesion of the photoresist layer to the substrate surface.

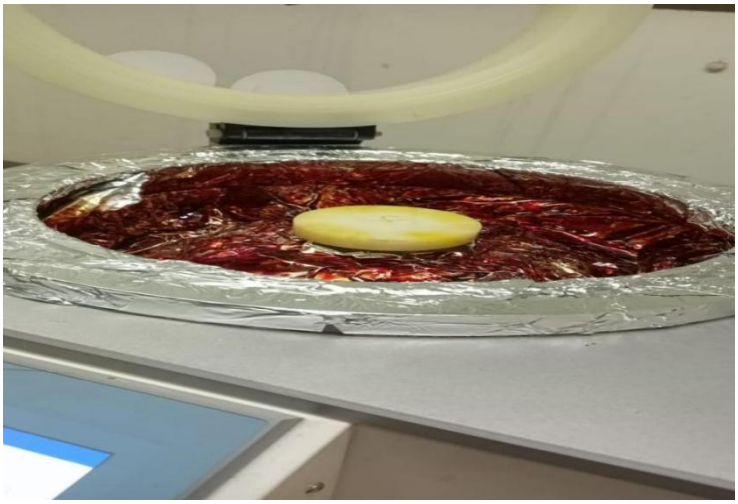

Figure 11:Spin coated

Step 2: Re-coating

A second layer of S1818 photoresist was applied to the wafer.

The spin-coating process was carried out at 3000 rpm for 30 seconds with an acceleration of 200 rpm/s to achieve a uniform and thin layer.

The coated wafer was prebaked at 95°C for 35 minutes to eliminate excess solvent and harden the photoresist slightly.

Purpose: - The prebaking steps ensured uniformity and improved adhesion of the photoresist, reducing the likelihood of defects during subsequent processing.

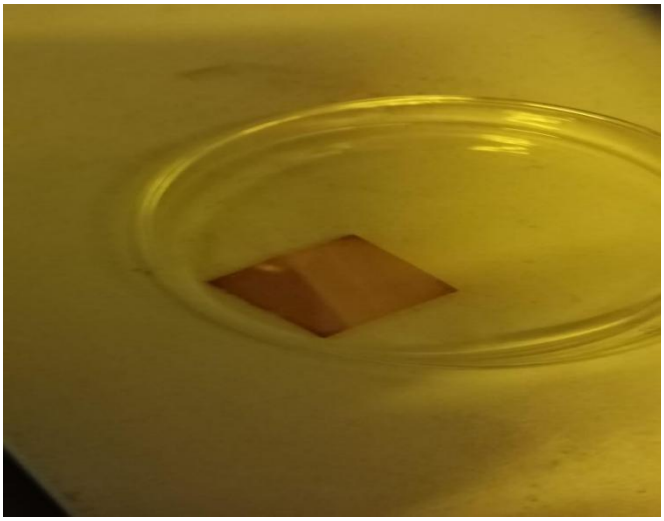

Figure 12:After spin coater

4.3.2 Exposure:

The wafer was exposed to a light source with a wavelength of 407 nm (near-UV range) and an intensity of 6.0 mW/cm².

A bright-field mask was used to define the desired pattern for the photoresist.

The exposure was performed for a total of 30 seconds, divided into two intervals of 18 seconds each, to minimize the risk of overexposure or damage.

Purpose:

The exposure transferred the mask pattern onto the photoresist by selectively breaking down the material in the exposed regions, as the S1818 photoresist is positive.

4.3.3 Development:

The exposed wafer was immersed in CD-26 developer (an alkaline developer for positive photoresists) for 70 seconds.

The wafer was then rinsed thoroughly with DI (deionized) water for 1–2 minutes to remove any residual developer.

Purpose:

The developer dissolved the exposed photoresist, Pattern matching with the Dark area of the mask.

4.3.4 Post-Baking

The developed wafer was baked at 97°C for 30 minutes.

Purpose:

This post-baking step hardened the remaining photoresist, improving its mechanical stability

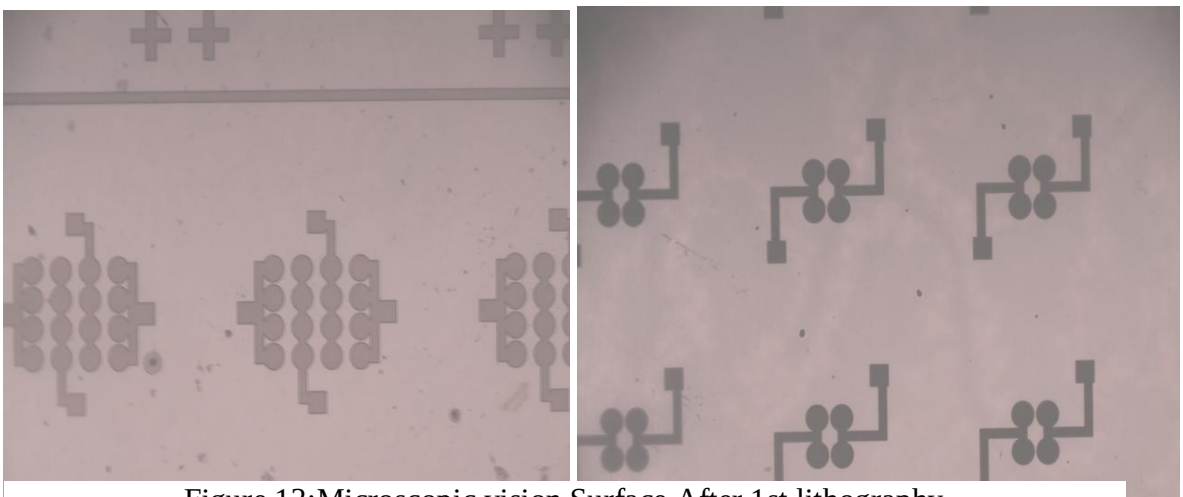

Figure 13:Microscopic vision Surface After 1st lithography

and resistance to subsequent etching steps.

4.3.5 Procedure for Mesa Etching Using an ICP-RIE Machine

4.3.5.1 Objective

To etch through the p-GaN, InGaN/GaN superlattice, and n-GaN layers to create a mesa structure with a total etch depth of 420 nm.

4.3.5.2 Equipment and Materials

ICP-RIE (Inductively Coupled Plasma - Reactive Ion Etching) machine

Process gases: BCl_3, Cl_2, and Ar

Sapphire epitaxy wafer with multilayer structure

Profilometer for depth measurement

4.3.5.3 Procedure

4.3.5.3.1 System Preparation

The ICP-RIE machine was powered on, and the chamber was cleaned to ensure no contamination from previous processes.

The temperature was set to 5°C, and the machine was allowed to stabilize.

The required gases (BCl_3, Cl_2, and Ar) were connected and flow rates verified.

4.3.5.3.2 Wafer Loading

The sapphire epitaxy wafer was mounted securely on the wafer holder inside the ICP-RIE chamber.

The chamber was sealed, and a vacuum was created to achieve the desired base pressure.

4.3.5.3.3 Process Setup

The process gases were introduced at the following flow rates:

BCl_3: 10 sccm

Cl_2: 32 sccm

Ar: 5 sccm

The RIE and ICP power settings were configured as follows:

RF Power: 30 W (biasing the wafer for anisotropic etching)

ICP Power: 300 W (generating high-density plasma for efficient etching)

The chamber pressure was adjusted to 5 Pa, and the system was allowed to stabilize for uniform plasma generation.

4.3.5.3.4 Etching Process

The etching process was initiated, and the wafer was exposed to the plasma for 5 minutes.

Real-time monitoring was conducted through the machine interface to ensure stable gas flow, power levels, and chamber pressure throughout the process.

4.3.5.3.5 Wafer Unloading

After the etching process, the plasma was extinguished, and the chamber was vented to atmospheric pressure.

The wafer was carefully removed using tweezers, avoiding damage to the etched structure.

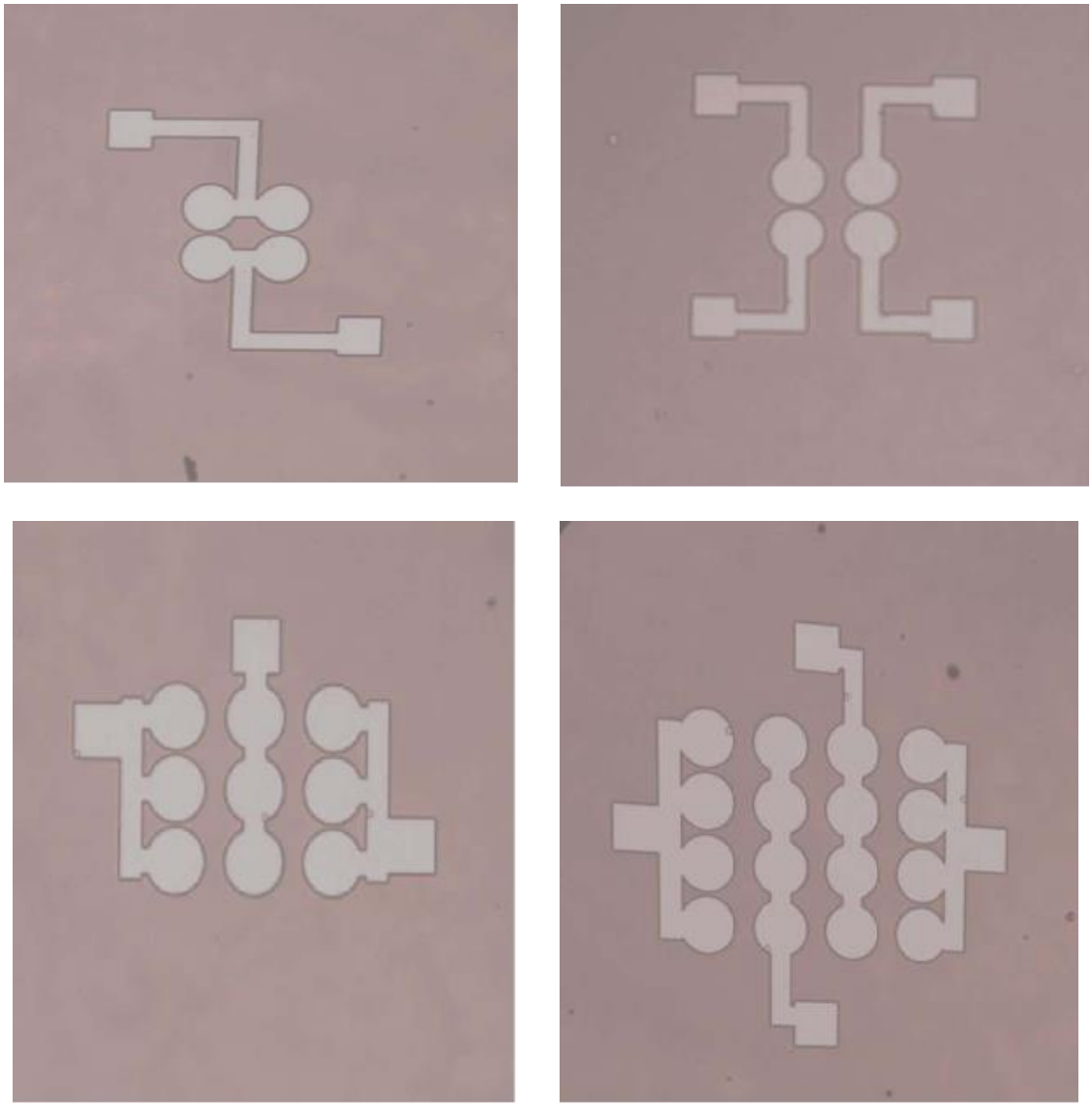

Figure 14:Microscopic vision after mesa etching

4.3.5.4 Post-Processing and Measurements

The etched wafer was inspected under an optical microscope for pattern fidelity and uniformity.

The etch depths were measured at multiple locations using a profilometer, yielding the following results:

Location 1: 851 nm at 6 mins

Location 2: 809 nm at 6 mins

Location 2: 529 nm at 5 mins

Location 2: 521 nm at 5 mins

4.3.5.5 Cleaning Process

Objective: To remove excess metal and photoresist after mesa etch.

Step 1: Soaking & Photoresist Removal

Non-LOR Photoresist Removal:

The wafer was immersed in acetone and soaked for 2 days to dissolve the standard S1818 photoresist.

Step 2: Sequential Cleaning

Q-tip Cleaning: The wafer was gently scrubbed with a Q-tip dipped in acetone.

Boiling Acetone:The wafer was immersed in boiling acetone (200°C) for 10 minutes.

IPA Bath:The wafer was then transferred to isopropyl alcohol (IPA).

Final Drying:The wafer was dried using N_2 gas to prevent contamination.

4.3.5.6 Procedure to Calculate Etch Depth Using a Profilometer

To determine the etch depth after etching through the p-GaN, InGaN/GaN superlattice, and n-GaN layers for a mesa structure (420 nm total depth), the following steps were performed:

4.3.5.6.1 Performing the Measurement

The stylus was aligned to scan across the etched and unetched regions of the mesa structure.The profilometer scan was started, allowing it to capture the step profile.The scan was ensured to include both the etched region i.e N type GaN (mesa bottom) and unetched region i.e P type GaN (mesa top).

4.3.5.6.2 Extracting Etch Depth

The etched region i.e N type GaN(lower level) and the unetched region i.e P type GaN (higher level) were identified.The vertical step height difference between these two regions was measured. The measured etch depth values were 851 nm, 575 nm, 591 nm and 529 nm.

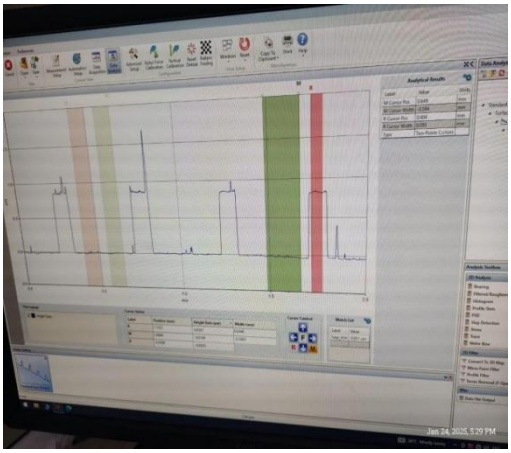

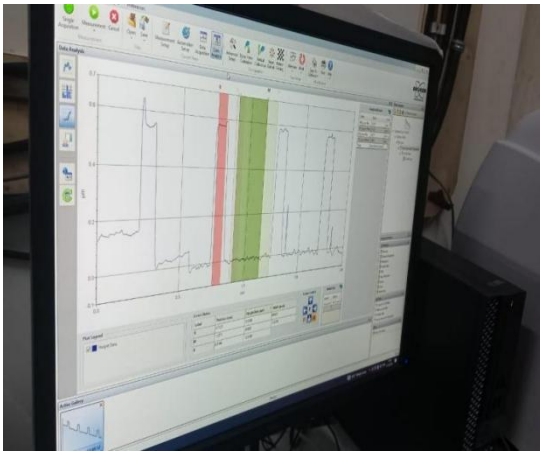

Figure 15:Profilometer etch depth measurement

4.3.5.7 Procedure for I-V Characteristics Measurement to ensure etching was done perfectly Using a 2-Probe System

4.3.5.7.1 Connecting the Device

The sample was placed on the probe station under a microscope for precise positioning.

The two probes were carefully positioned on the anode (p-side) to N-type GaN and cathode (n-side) to N-type GaN of the photodetector.

The fine adjustment knobs were used to gently touch the device contacts without damaging them.

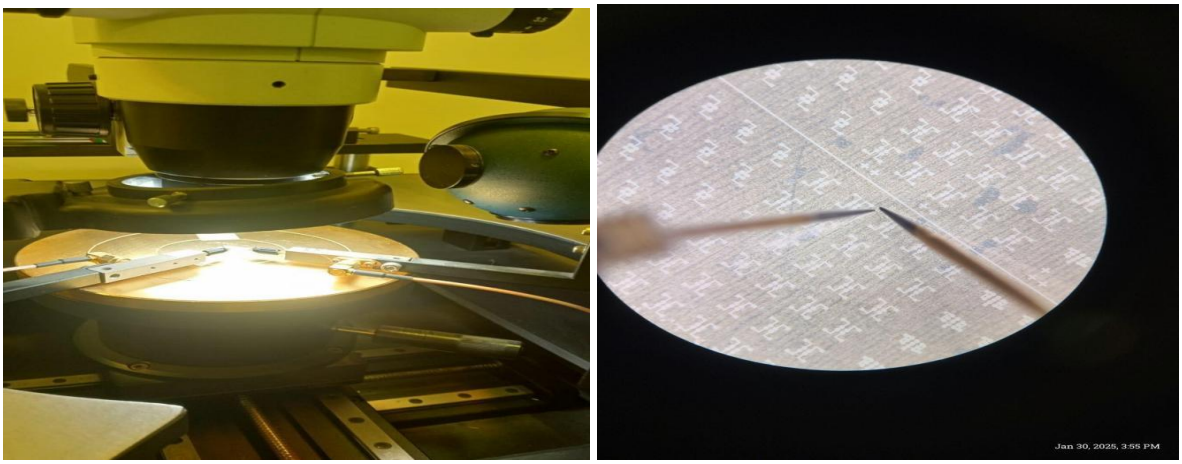

Figure 16:Microscopic vision I-V Characteristics Measurement to ensure etching.

4.3.5.7.2 Setting Up the Measurements

The voltage range was set from -5V to +10V.

The current measurement mode was chosen in microamps for photodetectors.

A 50-step size was selected for the voltage sweep.

The corresponding current was recorded for each voltage step.

4.3.5.7.3 Plotting the I-V Curve

The collected data was saved in an Excel file.The current (I) vs. voltage (V) was plotted using software like the LED Chip tester.

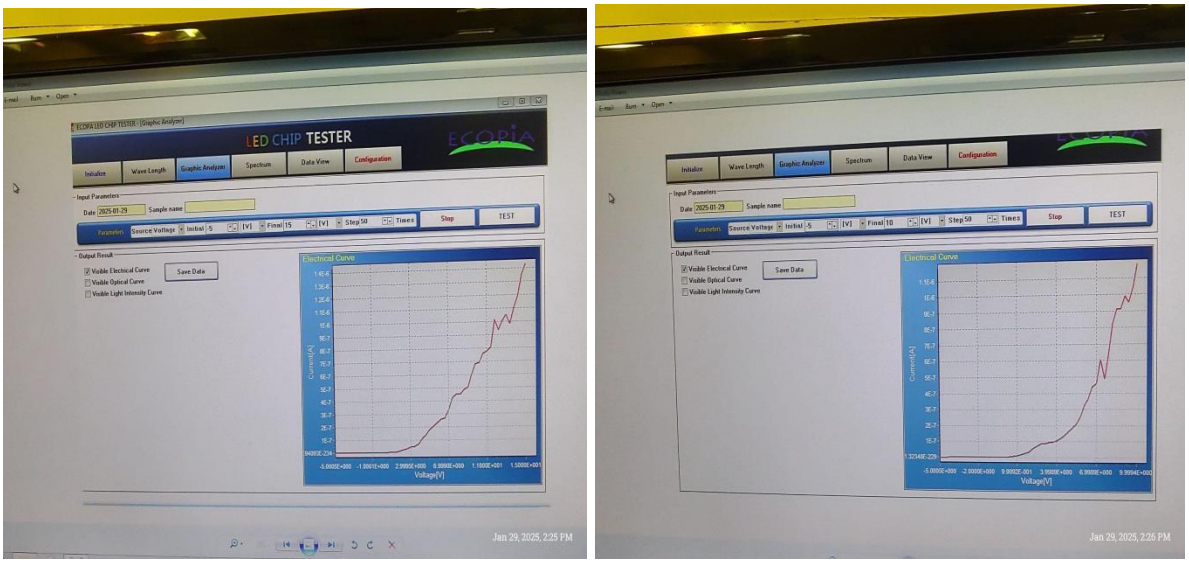

Figure 17: I-V Characteristics

The measurement showed a current of **1.1 µA at 10V**, confirming that the mesa etching was done

successfully.

4.3.6 N- Contact Deposition

4.3.6.1 Second-Level Lithography for N- Contact Deposition

Objective: To prepare the wafer for further processing, including metallization.

4.3.6.1.1 Spin coating

Step 1: Initial Coating

The S1818 photoresist was applied to the Glass wafer.

The Glass wafer was spin-coated initially at 1000 rpm for 10 seconds with an acceleration rate of 200 rpm/s to ensure an even spread of the photoresist across the surface to mount the Sapphire wafer.

Following this, the wafer was baked at 100℃ for 30 minutes to enhance the adhesion of the photoresist layer to the Sapphire substrate surface.

Step 2: Re-coating

A Second layer of " Lift-Off Resist (LOR)" was applied to the wafer.

The spin-coating process was carried out at 4500 rpm for 40 seconds with an acceleration of 200 rpm/s to enhance the lift-off process and improve the quality of metal deposition.

The coated wafer was prebaked at 150℃ for 30 minutes to eliminate excess solvent.

The prebaking steps ensured uniformity and improved adhesion of the photoresist, reducing the likelihood of defects during subsequent processing.

Step 3: Re-coating

A Third layer of S1818 photoresist was applied to the wafer.

The spin-coating process was carried out at 3000 rpm for 40 seconds with an acceleration of 200 rpm/s to achieve a uniform and thin layer.

The coated wafer was prebaked at 90℃ for 25 minutes to eliminate excess solvent and harden the photoresist slightly.

4.3.6.1.2 Exposure

The wafer was exposed to a light source with a wavelength of 407 nm (near-UV range) and an intensity of 6.0 mW/cm^2.

A Dark-field mask was used to define the desired pattern for the photoresist.

The exposure was performed for a total of 30 seconds.

Mask Type: Dark-Field Mask (the mask exposed light over the N-contact regions, while the surrounding areas are blocks).

Purpose:

The positive photoresist is weakened in exposed areas, allowing selective removal during development.

4.3.6.1.3 Development

The exposed wafer was immersed in CD-26 developer (an alkaline developer for positive photoresists) for 2 minutes.

The wafer was then rinsed thoroughly with DI (deionized) water for 2-3 minutes to remove any residual developer.

Purpose:

The developer intact the unexposed photoresist, Pattern matching with the Transparent area of the mask.

4.3.6.1.4 Pre-Baking

The developed wafer was baked at 90°C for 30 minutes. Purpose:

This pre-baking step hardened the remaining photoresist, improving its mechanical stability and resistance to Pre metallization etching steps.

Chemical Etching Procedure for Pre-Metallization Etch

Objective:

The objective was to remove surface oxides, contaminants, and residues from the wafer surface, ensuring a clean and well-adhered contact region before metallization.

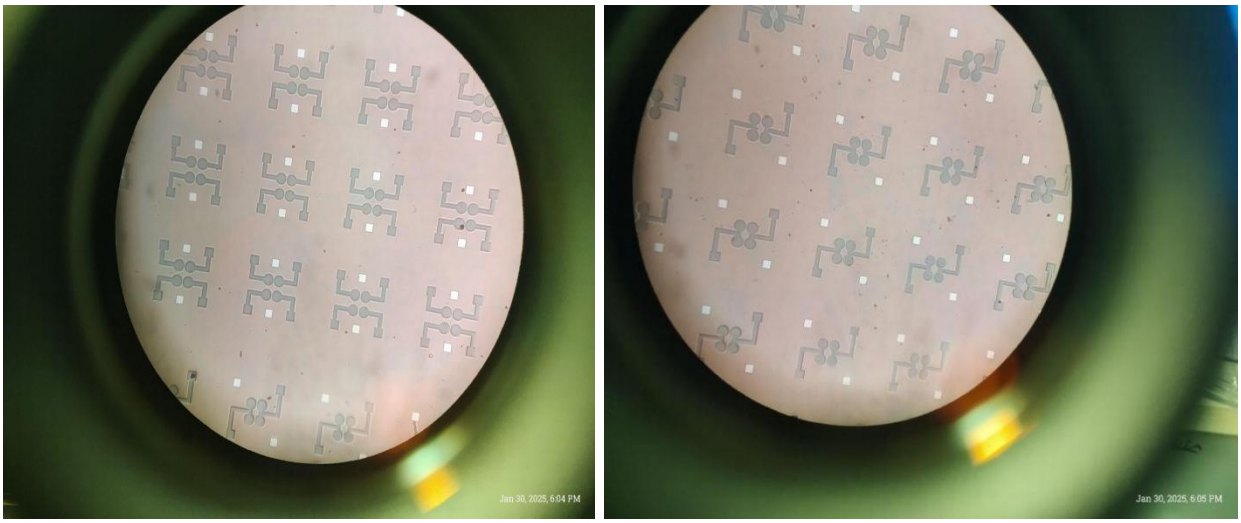

Figure 18:Microscopic vision after N- Contact lithography

4.3.6.2 Pre-metalization Etch by Chemical etching

Step 1. Preparation of the Etching Solution

Chemical Used: Hydrochloric Acid (HCl) and Deionized (DI) Water.

Solution Ratio: 1:1 ($HCl:H_2O$).

Preparation:

HCl was poured into a chemically resistant beaker.

An equal volume of DI water was added slowly to avoid splashing.

The solution was stirred gently to ensure uniform mixing.

Step 2. Wafer Etching Process

Wafer Handling:

Using clean, non-contaminating tweezers, the wafer was carefully placed into the prepared solution.

The wafer was fully submerged to ensure uniform etching.

Etching Time:

The wafer was maintained in the etching solution for 1 minute to effectively remove native oxides.

Step 3. Post-Etching Cleaning

Vigorous DI Water Rinse:

The wafer was immediately transferred into a DI water bath to remove any residual acid.

It was rinsed thoroughly for 1 minute to ensure the complete removal of acidic residues.

Nitrogen (N_2) Drying:

The wafer was dried using a N_2 gas gun to prevent water spots and contamination.

4.3.6.3 Metallization of N-Contact Using Electron Beam Deposition

Objective:

The objective was to deposit metal layers (Ti/Al/Ni/Au) to form n-type electrical contacts on the device surface.

Step 1: Loading the Samples

The samples were mounted onto the substrate holder inside the E-beam chamber.

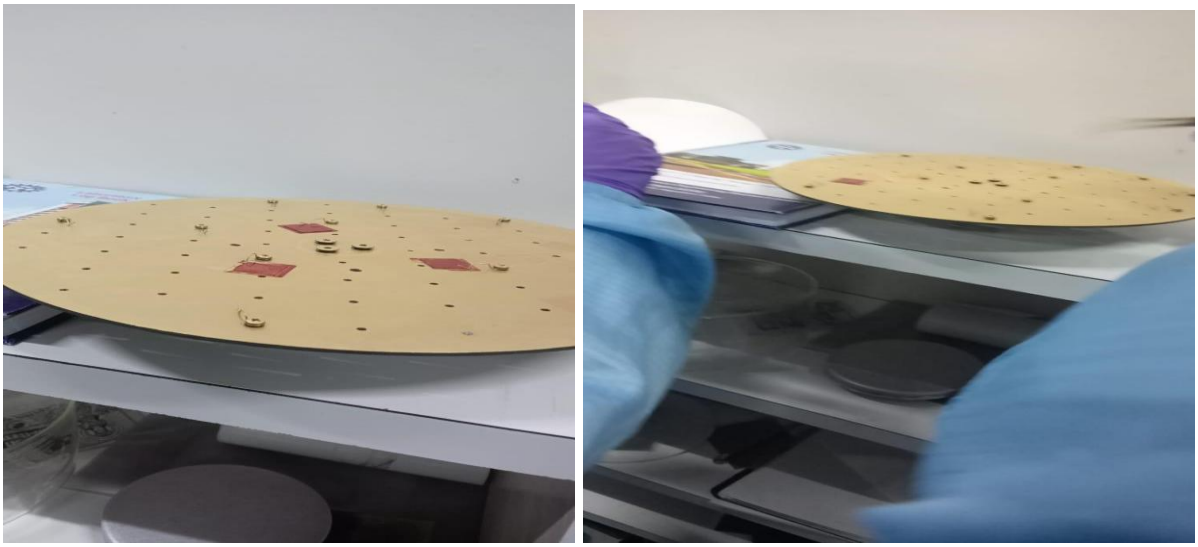

Figure 19:Loading the wafer on the chamber

Step 2: Vacuum Setup

The chamber was pumped down to achieve a vacuum of $< 10^{-6}$ Torr before deposition.

Step 3: Metal Deposition Process (Ti/Al/Ni/Au - 30/100/20/100 nm)

Titanium (Ti) Deposition – 30 nm

Purpose: Improved adhesion between the contact metal and semiconductor surface.

Aluminum (Al) Deposition – 100 nm

Purpose: Acted as the primary n-contact material for low-resistance ohmic contact.

Nickel (Ni) Deposition – 20 nm

Purpose: Served as a diffusion barrier to prevent intermixing of Al and Au layers.

Gold (Au) Deposition – 100 nm

Purpose: Provided a stable and conductive top layer, enhancing the contact's durability.

Step 4: Cooling

The chamber was allowed to cool down before venting to prevent oxidation.

Figure 20: Remove the wafers After N-Contact deposition from the chamber.

4.3.6.4 N-Contact Lift-off

Objective: To remove excess metal and photoresist after electron beam deposition.

Step 1: Soaking & Photoresist Removal

Non-LOR Photoresist Removal:

The wafer was immersed in acetone and soaked for 3 days to dissolve the standard S1818 photoresist.

Lift-Off Resist (LOR) Removal:

The wafer was immersed in a PG remover for 3 days to break down the LOR layer.

Step 2: Ultrasonic Cleaning

The wafer was placed in an ultrasonic bath filled with acetone.

Duration:370 seconds at 200°Cto break off residual metal.

Step 3: Sequential Cleaning

Q-tip Cleaning:

The wafer was gently scrubbed with a Q-tip dipped in acetone.

Boiling Acetone:

The wafer was immersed in boiling acetone (200°C) for 10 minutes.

IPA Bath:

The wafer was then transferred to isopropyl alcohol (IPA).

Final Drying:

The wafer was dried using N_2 gas to prevent contamination.

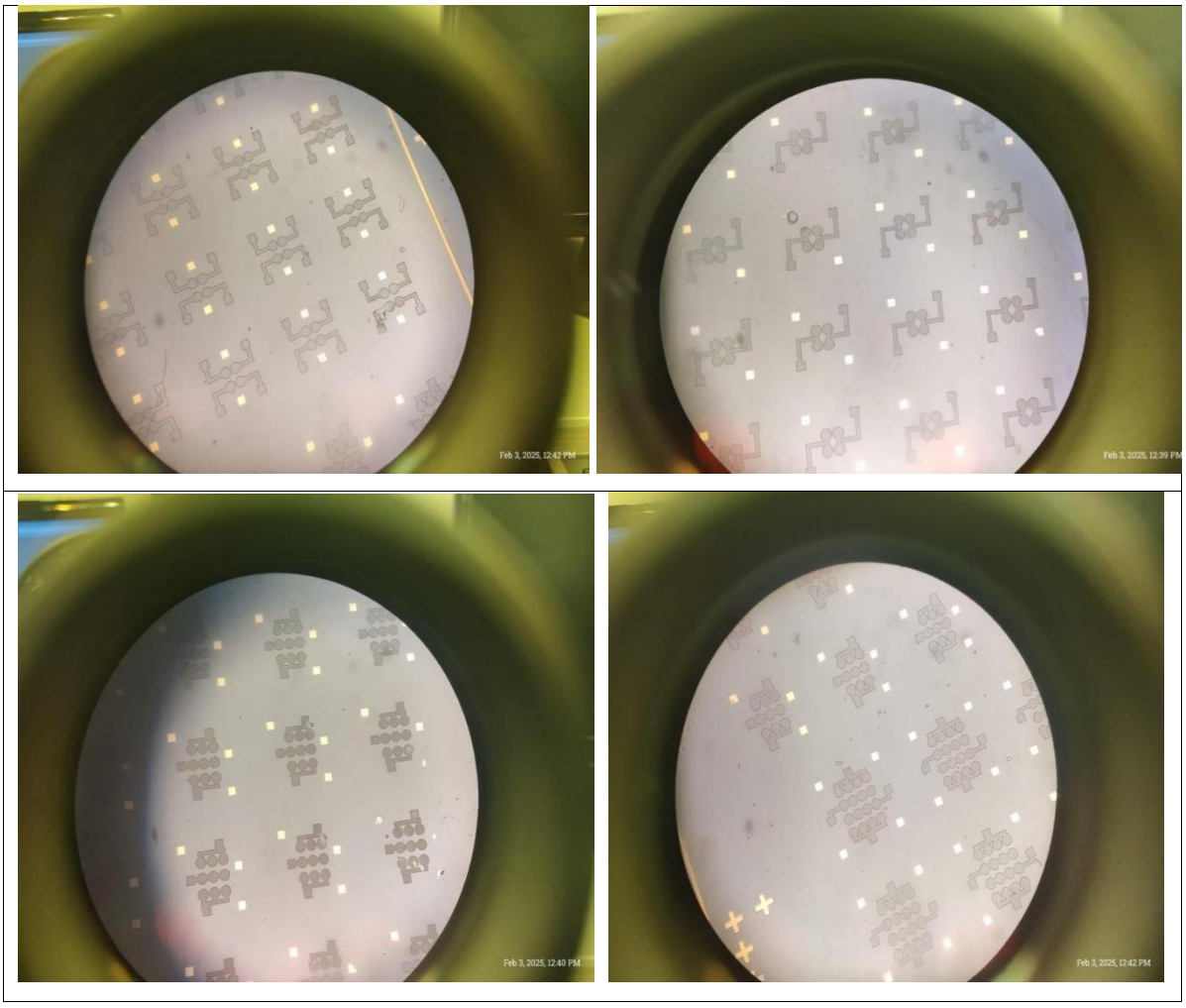

Figure 21:Microscopic vision after N- Contact Deposition

4.3.6.5 Annealing Using Rapid Thermal Annealing (RTA)

Objective: To improve the electrical contact quality and adhesion of the Ti/Al/Ni/Au stack on n-GaN.

Step 1: Wafer Loading

The wafer was loaded onto the quartz holder inside the chamber.

Step 2: Gas Flow Setup

Nitrogen (N_2) flow:150 sccm (to prevent oxidation).

Step 3: Heating Profile

Ramp-up:

The temperature was increased to 815°Cwithin 25 seconds.

Hold Time:

The wafer was maintained at 815°Cfor 30 seconds.

Cool-down:

The system was slowly cooled down under N_2 flow to avoid thermal stress.

Step 4: Wafer Removal

Once cooled, the wafer was carefully removed and inspected under an optical microscope.

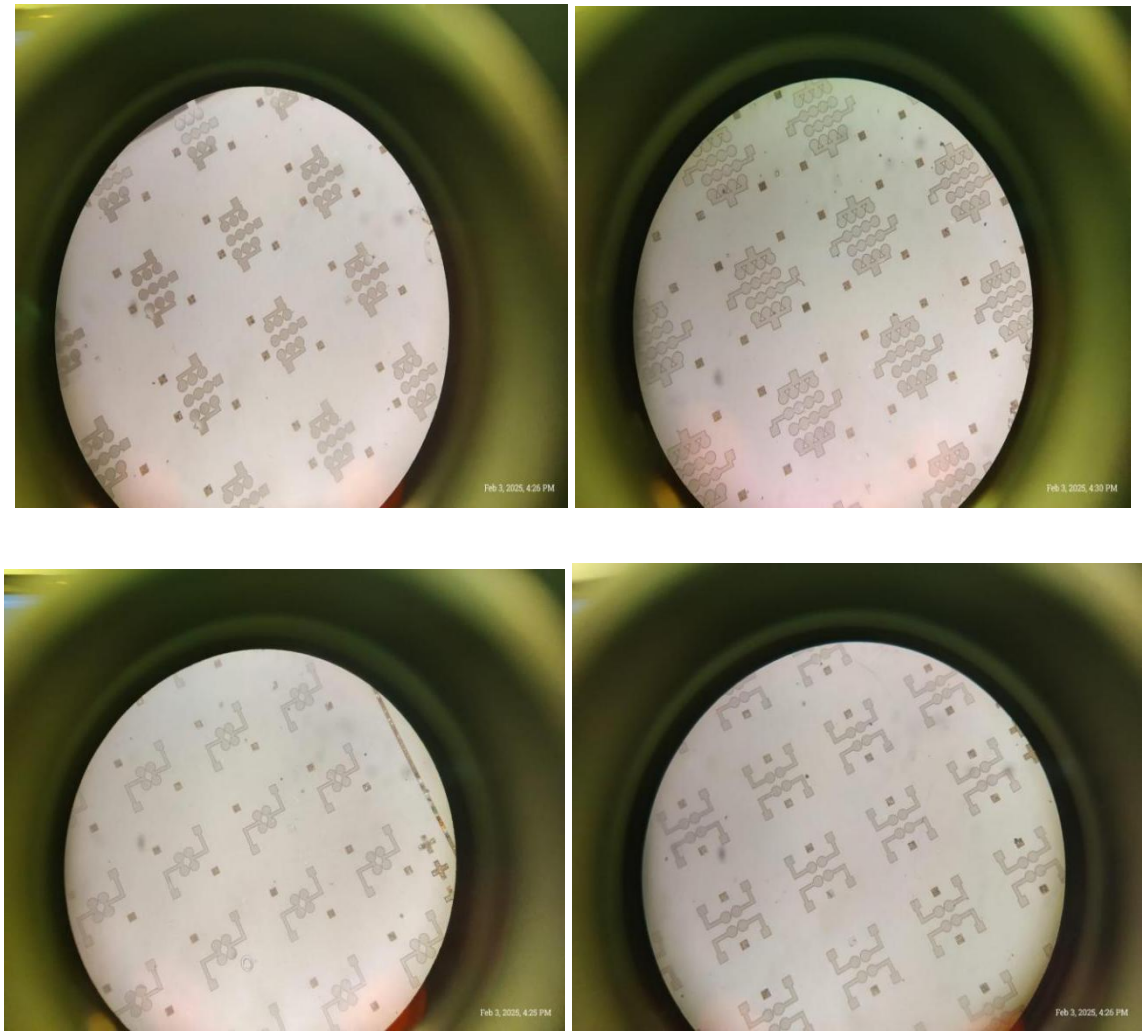

Figure 22:Microscope image N Contact Annelling.

The Beakers, Boat and Pattern disk was cleaned with IPA.

4.3.7 ITO Deposition.

4.3.7.1 Third-Level Lithography for ITO Deposition.

Objective: To prepare the wafer for further processing, including ITO Deposition.

4.3.7.1.1 Spin coating

Step 1: Initial Coating

The S1818 photoresist was applied to the Glass wafer.

The Glass wafer was spin-coated initially at 1000 rpm for 30 seconds with an acceleration rate of 200 rpm/s to ensure an even spread of the photoresist across the surface to mount the

Sapphire wafer.

Following this, the wafer was baked at 120℃ for 15 minutes to enhance the adhesion of the photoresist layer to the Sapphire substrate surface.

Step 2: Re-coating

A Second layer of " Lift-Off Resist (LOR)" was applied to the wafer.

The spin-coating process was carried out at 4500 rpm for 40 seconds with an acceleration of 200 rpm/s to enhance the lift-off process and improve the quality of metal deposition.

The coated wafer was prebaked at 150℃ for 35 minutes to eliminate excess solvent.

Purpose:

The prebaking steps ensured uniformity and improved adhesion of the photoresist, reducing the likelihood of defects during subsequent processing.

Step 3: Re-coating

A second layer of S1818 photoresist was applied to the wafer.

The spin-coating process was carried out at 3500 rpm for 30 seconds with an acceleration of 200 rpm/s to achieve a uniform and thin layer.

The coated wafer was prebaked at 90℃ for 25 minutes to eliminate excess solvent and harden the photoresist slightly.

4.3.7.1.2 Exposure

The wafer was exposed to a light source with a wavelength of 407 nm (near-UV range) and an intensity of 6.0 mW/cm^2.

A Dark-field mask was used to define the desired pattern for the photoresist.

The exposure was performed for a total of 23 seconds.

Mask Type: Dark-Field Mask (the mask exposed light over the ITO regions, while the surrounding areas are blocks).

Purpose:

The positive photoresist is weakened in exposed areas, allowing selective removal during development.

4.3.7.1.3 Development

The exposed wafer was immersed in CD-26 developer (an alkaline developer for positive

photoresists) for 75 Sec.

The wafer was then rinsed thoroughly with DI (deionized) water for 2-3 minutes to remove any residual developer.

Purpose:

The developer intact the unexposed photoresist, Pattern matching with the Transparent area of the mask.

4.3.7.1.4 Post-Baking

The developed wafer was baked at 100°C for 25 minutes.

Purpose:

This post-baking step hardened the remaining photoresist, improving its mechanical stability and resistance to Pre metallization etching steps.

Chemical Etching Procedure for Pre-Metallization Etch

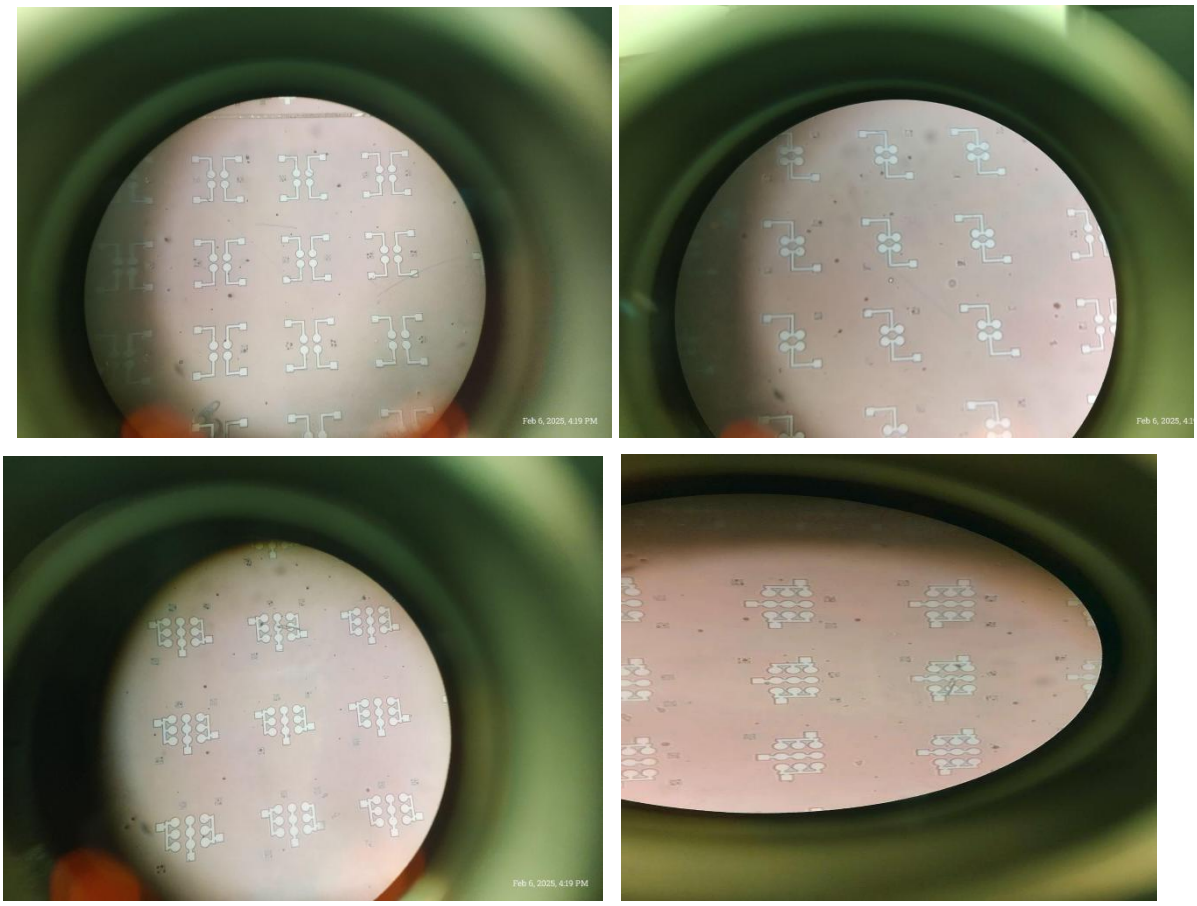

Figure 23: Microscope image after ITO lithography

Objective:

The objective was to remove surface oxides, contaminants, and residues from the wafer surface, ensuring a clean and well-adhered contact region before metallization.

4.3.7.2 Plasma etching:

Objective: To remove excess photoresist on the ITO surface after lithography.

Step 1. Chamber Setup: The plasma etching system was powered on, and the required parameters were set. The RF power was adjusted to 100 watts, and the etching duration was configured for 2 minutes.

Step 2. Gas Introduction: A controlled flow of O_2 gas was introduced into the chamber to facilitate the etching process.

Step 3. Plasma Generation: The RF power supply was activated, generating plasma within the chamber. The sample was exposed to the plasma, where the reactive ions selectively etched the ITO material.

Step 4. Monitoring: The etching process was closely monitored to ensure uniformity and to prevent over-etching of the ITO layer.

Step 5. Completion**:** After 2 minutes, the plasma was deactivated, and the gas flow was stopped.

Step 6. Post-Etching Cleaning: The sample was removed from the chamber and examined under a microscope to assess the etching quality. Any residual material was cleaned as required.

4.3.7.3 Pre-metalization Etch by Chemical etching

Step 1. Preparation of the Etching Solution

Chemical Used: Hydrochloric Acid (HCl) and Deionized (DI) Water.

Solution Ratio: 1:1 ($HCl:H_2O$).

Preparation:

HCl was poured into a chemically resistant beaker.

An equal volume of DI water was added slowly to avoid splashing.

The solution was stirred gently to ensure uniform mixing.

Step 2. Wafer Etching Process

Wafer Handling:

Using clean, non-contaminating tweezers, the wafer was carefully placed into the prepared solution.

The wafer was fully submerged to ensure uniform etching.

Etching Time:

The wafer was maintained in the etching solution for 1 minute to effectively remove native oxides.

Step 3. Post-Etching Cleaning

Vigorous DI Water Rinse:

The wafer was immediately transferred into a DI water bath to remove any residual acid.

It was rinsed thoroughly for 1 minute to ensure the complete removal of acidic residues.

Nitrogen (N_2) Drying:

The wafer was dried using a N_2 gas gun to prevent water spots and contamination.

4.3.7.4 ITO Deposition Using Electron Beam Deposition

Objective:

The goal was to deposit a 100 nm layer of Indium Tin Oxide (ITO) to create transparent conductive electrodes on both wafers and glass substrates, enabling the evaluation of thickness, resistivity, and transmittance.

Method: Electron Beam Deposition (E-Beam Evaporation) was used to deposit the ITO layer.

Step 1. Vacuum Chamber Setup:

Wafers were loaded in the chamber.

The chamber was pumped down to a vacuum pressure of better than 10^{-6} Torr to minimize contamination.

The electron beam gun was calibrated and aligned with the ITO target material.

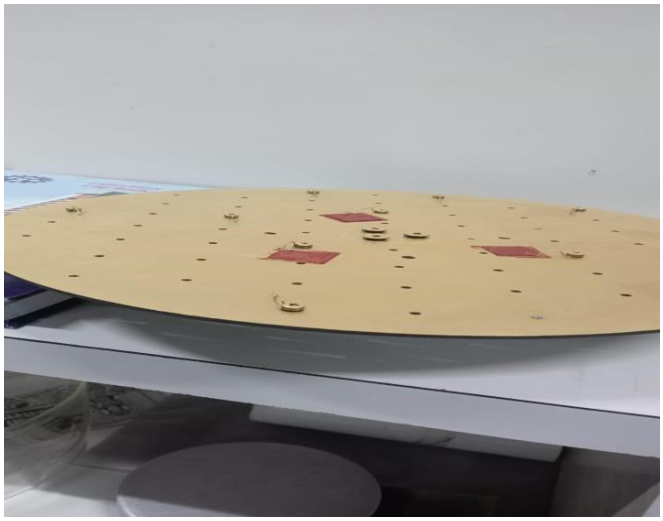

Figure 24:Wafer's loaded on the chamber

Step 2. Electron Beam Source Activation:

The electron beam power supply was set to 7.9 kV to generate the necessary energy for evaporating ITO.

Step 3. Deposition Process:

The deposition began at an initial rate of 0.2 Å/s at 8% power to ensure uniform nucleation.

The power was gradually increased to 10%, maintaining the deposition rate at 0.2 Å/s.

Step 4. Completion and Cooling:

Once the 100 nm thickness was achieved, the electron beam was turned off, and the system was allowed to cool gradually.

The chamber pressure was stabilized before venting.

Step 5. Sample Unloading:

The Wafer was carefully removed from the chamber using clean tweezers.

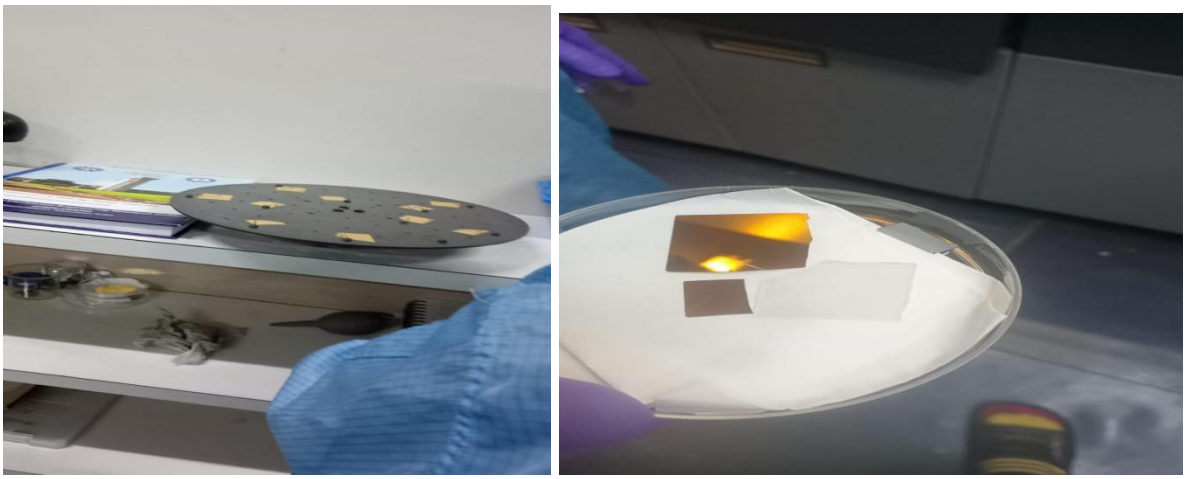

Figure 25: Wafer's removed after ITO Deposition.

4.3.7.5 ITO Lift-off

Objective: To remove Photoresist and LOR after electron beam deposition.

Step 1: LOR Removal

Lift-Off Resist (LOR) Removal:

Boiling LOR :

The wafer was immersed in boiling PG remover (200°C) for 10 minutes.

The wafer was immersed in a PG remover for 4 Hours to break down the LOR layer.

Step 2: Sequential Cleaning

Q-tip Cleaning:

The wafer was gently scrubbed with a Q-tip dipped in acetone.

Boiling Acetone:

The wafer was immersed in boiling acetone (200℃) for 10 minutes.

IPA Bath:

The wafer was then transferred to isopropyl alcohol (IPA).

Final Drying:

The wafer was dried using N_2 gas to prevent contamination.

4.3.7.6 ITO Thickness measurement:

The thickness of the ITO layer, deposited via electron beam deposition, was measured using a profilometer and found to be 105 nm.

4.3.7.7 Annealing Using Rapid Thermal Annealing (RTA)

Objective: To improve the electrical contact quality and adhesion of the ITO on p-GaN.

Step 1: Wafer Loading

The wafer was loaded onto the quartz holder inside the chamber.

Step 2: Gas Flow Setup

Nitrogen (N_2) flow:150 sccm (to prevent oxidation).

Step 3: Heating Profile

Ramp-up:

The temperature was increased to 550°C within 15 seconds.

Hold Time:

The wafer was maintained at 550°C for 300 seconds.

Cool-down:

The system was slowly cooled down under N_2 flow to avoid thermal stress.

Step 4: Wafer Removal

Once cooled, the wafer was carefully removed and inspected under an optical microscope.

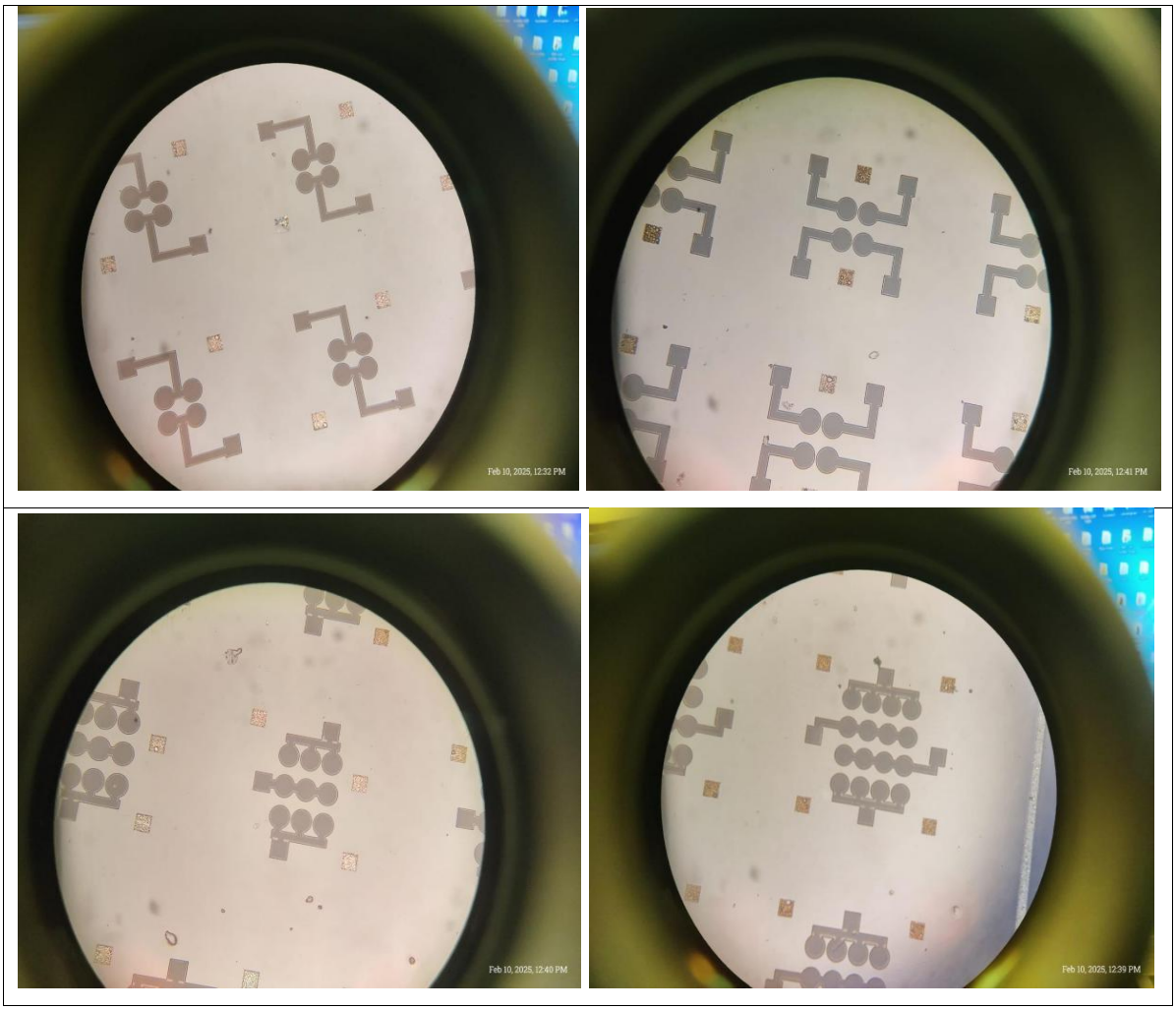

Figure 26:Microscope image after ITO Annealing.

4.5.8 Four-Point Probe Method for Resistivity Measurement Objective:

To determine the sheet resistance (Ω/square) of the ITO-deposited glass wafer before and after annealing.

Procedure:

The ITO-coated glass wafer was placed on the measurement stage.

Proper electrical contact was ensured without damaging the wafer surface.

A constant voltage was applied to the probes.

Results Recording:

The resistivity values before and after annealing were recorded:

Before annealing: 480 Ω/square

After annealing: 118.2 Ω/square

Figure 27:Resistivity Measured byFour-Point Probe Method

4.3.7.8 Spectrophotometer Measurement of Transmittance

Objective:

To evaluate the optical transmittance of the ITO-coated glass wafer over the wavelength range of 200 nm to 800 nm.

Procedure:

Step 1. System Setup:

The spectrophotometer was powered on and allowed to stabilize.

The transmittance mode was selected, and the measurement range was set from 200 nm to 800 nm.

Step 2. Baseline Calibration:

A blank (uncoated) glass wafer for reference was placed in the sample holder.

A baseline scan was performed, and the transmittance was recorded as a black line.

Step 3. Sample Measurement:

The blank glass wafer was replaced with the ITO-coated glass wafer before annealing.

Proper alignment in the sample holder was ensured.

A scan was conducted, and the transmittance was recorded as a blue line.

Figure 28:Transmittance of reference glass wafer represents black colour.

Figure 29:Transmittance of wafer before Annealing represents blue colour.

The pre-annealed wafer was then replaced with the ITO-coated glass wafer after annealing.

Accurate positioning in the sample holder was ensured.

A scan was performed, and the transmittance was recorded as a red line.

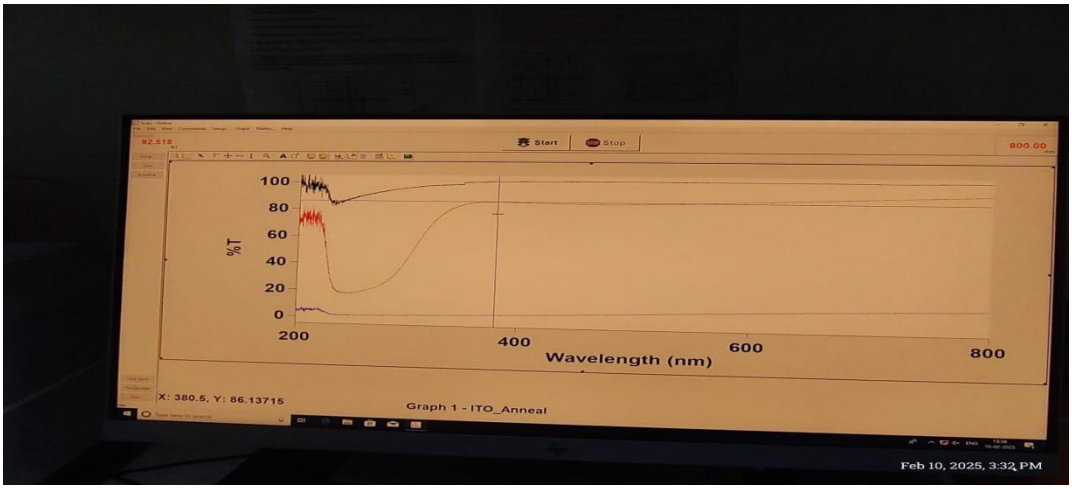

Figure 30:Transmittance of wafer After Annealing represents red colour.

Step 4. Results Recording:

The transmittance measured at 380 nm was approximately 86.13%.

The results were compared with reference i.e blank (uncoated) glass wafer values and Sumanth Sir's thesis on ITO coatings for quality verification.

4.3.8 Pads N type and P type Contact Deposition.

4.3.8.1 Fourth-Level Lithography for Pads N type and P type Contact Deposition.

Objective: Patterning for the next stage of both Pads N type and P type Contact Deposition.

4.6.1.1 Spin coating

Step 1: Initial Coating

The S1818 photoresist was applied to the Glass wafer.

The Glass wafer was spin-coated initially at 1000 rpm for 30 seconds with an acceleration rate of 200 rpm/s to ensure an even spread of the photoresist across the surface to mount the Sapphire wafer.

Following this, the wafer was baked at 120°C for 15 minutes to enhance the adhesion of the photoresist layer to the Sapphire substrate surface.

Step 2: Re-coating

A Second layer of " Lift-Off Resist (LOR)" was applied to the wafer.

The spin-coating process was carried out at 4500 rpm for 40 seconds with an acceleration of 200 rpm/s to enhance the lift-off process and improve the quality of metal deposition.

The coated wafer was prebaked at 150°C for 35 minutes to eliminate excess solvent.

Purpose:

The prebaking steps ensured uniformity and improved adhesion of the photoresist, reducing the likelihood of defects during subsequent processing.

Step 3: Re-coating

A second layer of S1818 photoresist was applied to the wafer.

The spin-coating process was carried out at 3500 rpm for 30 seconds with an acceleration of 200 rpm/s to achieve a uniform and thin layer.

The coated wafer was prebaked at 90°C for 25 minutes to eliminate excess solvent and harden the photoresist slightly.

4.3.8.1.1 Exposure

The wafer was exposed to a light source with a wavelength of 407 nm (near-UV range) and an intensity of 6.0 mW/cm².

A Dark-field mask was used to define the desired pattern for the photoresist.

The exposure was performed for a total of 23 seconds.

Mask Type: Dark-Field Mask (the mask exposed light over the both N type and P type contact's regions, while the surrounding areas are blocks).

Purpose:

The positive photoresist is weakened in exposed areas, allowing selective removal during development.

4.3.8.1.2 Development

The exposed wafer was immersed in CD-26 developer (an alkaline developer for positive photoresists) for 75 Sec.

The wafer was then rinsed thoroughly with DI (deionized) water for 2-3 minutes to remove any residual developer.

Purpose:

The developer intact the unexposed photoresist, Pattern matching with the Transparent area of the mask.

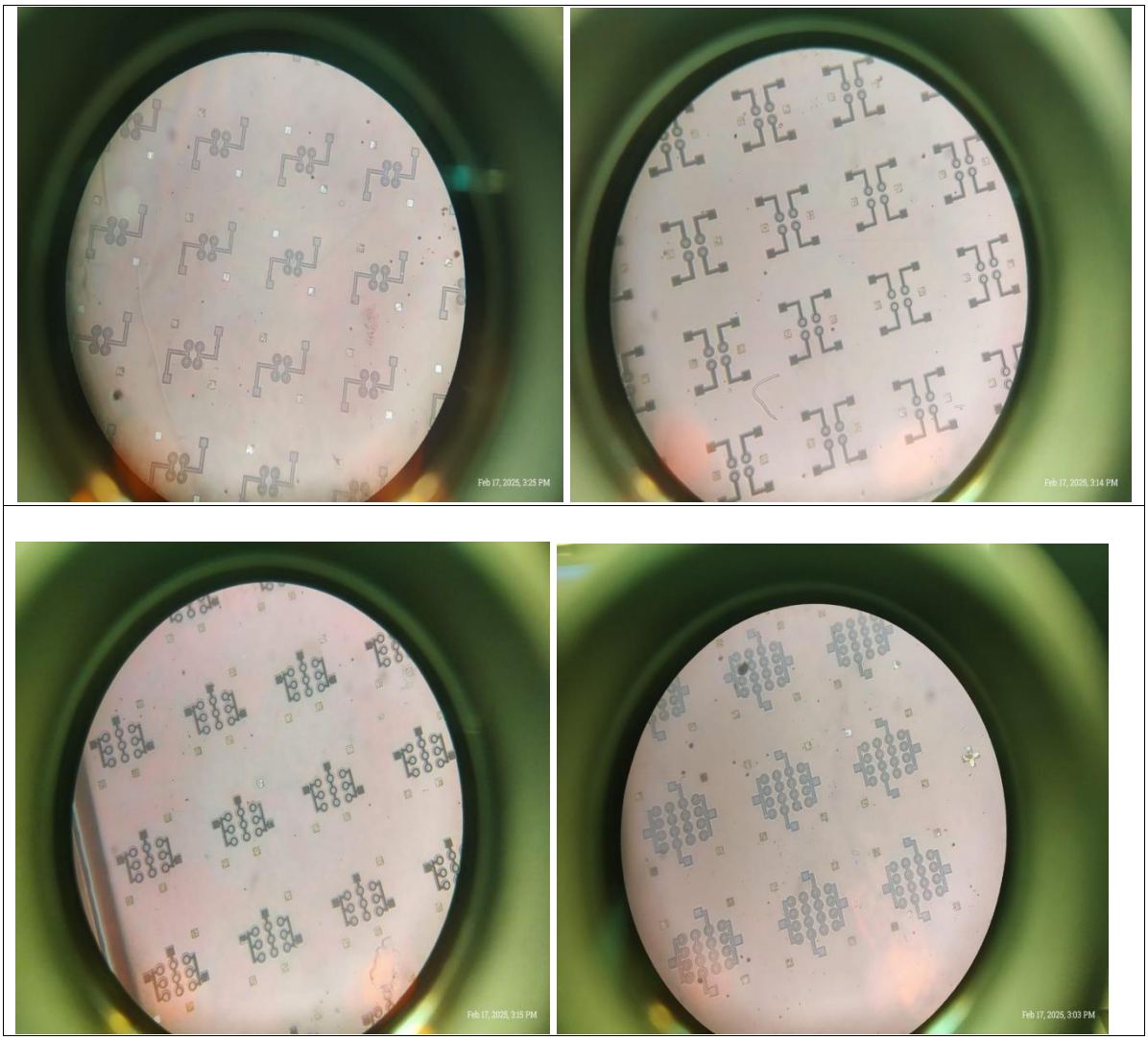

Figure 31:Microscope image the N-type and P-type after deposition lithography.

4.3.8.2 Plasma Ashing

Objective: The plasma ashing process was conducted to remove excess photoresist from the N-type and P-type pad surfaces after lithography.

Step 1. The sample was placed inside the plasma ashing chamber.

Step 2. The chamber was evacuated to achieve the required vacuum level.

Step 3. Oxygen gas was introduced into the chamber, maintaining a pressure of 400 Pascal.

Step 4. The plasma ashing system was operated at a power of 150 watts.

Step 5. The process was run for a duration of 2 minutes to ensure complete removal of the excess photoresist.

Step 6. After completion, the chamber was vented, and the sample was carefully removed.

Step 7. The sample was inspected under a microscope to confirm the successful removal of the photoresist.

4.3.8.3 Pre-Metallization Etch for Pad Contact Deposition

4.3.8.3.1 Preparation of the Etching Solution:

Step 1. A Teflon beaker was cleaned thoroughly with deionized (DI) water and dried to prevent contamination.

Step 2. Hydrofluoric acid (HF) was carefully poured into the Teflon beaker.

Step 3. DI water was added to the HF in a 1:30 ratio to prepare the etching solution.

Step 4. The solution was stirred gently to ensure uniform mixing.

4.3.8.3.2 Wafer Etching Process:

Step 1. The wafer was carefully dip into the prepared HF:H_2O solution.

Step 2. The etching process was carried out for 2-3 seconds to remove surface oxides and contaminants.

Step 3. The wafer was monitored closely to avoid over-etching.

4.3.8.3.3 Post-Etching Cleaning:

Step 1. After etching, the wafer was immediately transferred to a fresh Teflon beaker containing DI water for the rinsing process.

Step 2. A vigorous DI water rinse was performed for 10 minutes in flowing DI water to eliminate any residual acid.

Step 3. The wafer was then dried using a nitrogen gun to ensure a clean and moisture-free surface.

4.3.8.4 Pad Contact Metallization Procedure

Objective:

To deposit Ti/Au layers for n and p pad contacts using electron beam (E-beam) evaporation.

Step 1. Loading the Samples and Vacuum Setup:

The substrate was loaded into the E-beam evaporation chamber.

The chamber was evacuated to a vacuum level greater than 10^{-7} Torr.

Step 2. Titanium Deposition:

The E-beam power was set to 15%.

Deposition began with an initial rate of 0.2 Å/s for the first 20% of the total thickness (4 nm).

The deposition rate was gradually increased to 0.4 Å/s until a total thickness of 20 nm was achieved.

Step 3. Gold Deposition:

The E-beam power was adjusted to 12-14%.

Deposition started at an initial rate of 0.2 Å/s for the first 20% of the total thickness (10 nm).

The deposition rate was increased to 0.4 Å/s until the final thickness of 50 nm was reached.

Step 4. Cooling:

The deposited layers were allowed to cool down in a controlled vacuum environment.

The substrate was carefully removed from the chamber.

Figure 32:After N and P Pad Contact Deposition removed wafer from chamber.

4.3.8.5 N and P Pad Contact Liftoff

Objective: To remove excess metal and photoresist after electron beam deposition.

Step 1: Soaking & Photoresist Removal

Lift-Off Resist (LOR) Removal:

The wafer was immersed in a PG remover for 2 days(4 hours enough) to break down the LOR layer.

Step 2: Ultrasonic Cleaning

The wafer was placed in an ultrasonic bath filled with acetone.

Duration:300 seconds at 200°Cto break off residual metal.

Step 3: Sequential Cleaning

Q-tip Cleaning:

The wafer was gently scrubbed with a Q-tip dipped in acetone.

Boiling Acetone:

The wafer was immersed in boiling acetone (200℃) for 10 minutes.

IPA Bath:

The wafer was then transferred to isopropyl alcohol (IPA).

Final Drying:

The wafer was dried using N_2 gas to prevent contamination.

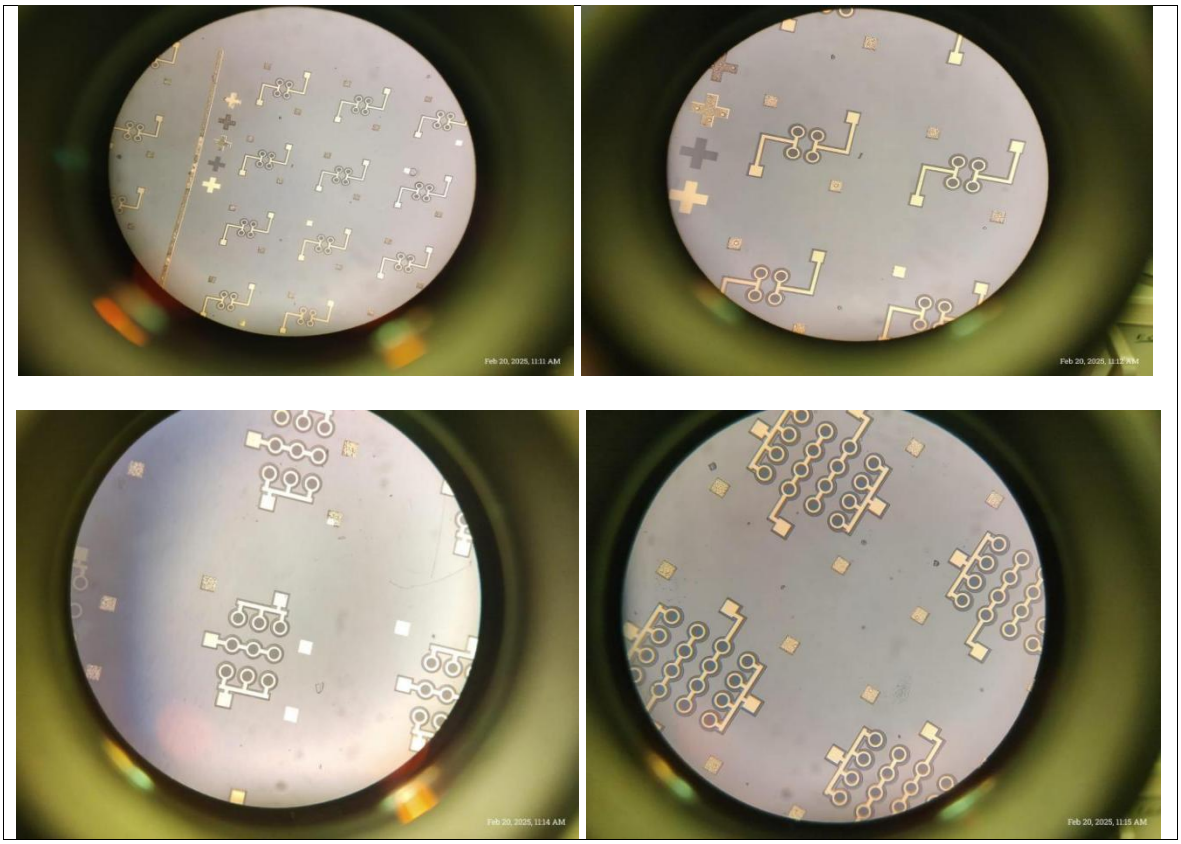

Figure 33:Microscope image after N and P Pad Contact Deposition.

4.3.9 Pads opening or Deposition of Passivation layer.

4.3.9.1 Fifth-Level Lithography for Pads opening or Deposition of Passivation layer.

Objective: Patterning for the next stage of Pads opening or Deposition of Passivation layer.

4.3.9.1.1 Spin coating

Step 1: Initial Coating

The S1818 photoresist was applied to the Glass wafer.

The Glass wafer was spin-coated initially at 1000 rpm for 30 seconds with an acceleration rate of 200 rpm/s to ensure an even spread of the photoresist across the surface to mount the Sapphire wafer.

Following this, the wafer was baked at 120℃ for 15 minutes to enhance the adhesion of the photoresist layer to the Sapphire substrate surface.

Step 2: Re-coating

A Second layer of " Lift-Off Resist (LOR)" was applied to the wafer.

The spin-coating process was carried out at 4500 rpm for 40 seconds with an acceleration of 200 rpm/s to enhance the lift-off process and improve the quality of metal deposition.

The coated wafer was prebaked at 150℃ for 35 minutes to eliminate excess solvent.

Purpose:

The prebaking steps ensured uniformity and improved adhesion of the photoresist, reducing the likelihood of defects during subsequent processing.

Step 3: Re-coating

A second layer of S1818 photoresist was applied to the wafer.

The spin-coating process was carried out at 3500 rpm for 30 seconds with an acceleration of 200 rpm/s to achieve a uniform and thin layer.

The coated wafer was prebaked at 90℃ for 25 minutes to eliminate excess solvent and harden the photoresist slightly.

4.3.9.1.2 Exposure

The wafer was exposed to a light source with a wavelength of 407 nm (near-UV range) and an intensity of 6.0 mW/cm².

A Briegt-field mask was used to define the desired pattern for the photoresist.

The exposure was performed for a total of 23 seconds.

Mask Type: Bright-Field Mask (the mask blocks light over the both N type and P type Pads regions, while the surrounding areas are exposed).

Purpose:

The positive photoresist is weakened in exposed areas, allowing selective removal during development.

4.3.9.1.3 Development

The exposed wafer was immersed in CD-26 developer (an alkaline developer for positive photoresists) for 3 mins.

The wafer was then rinsed thoroughly with DI (deionized) water for 2-3 minutes to remove any residual developer.

Purpose:

The developer dissolves the exposed photoresist, Pattern matching with the Dark area of the mask.

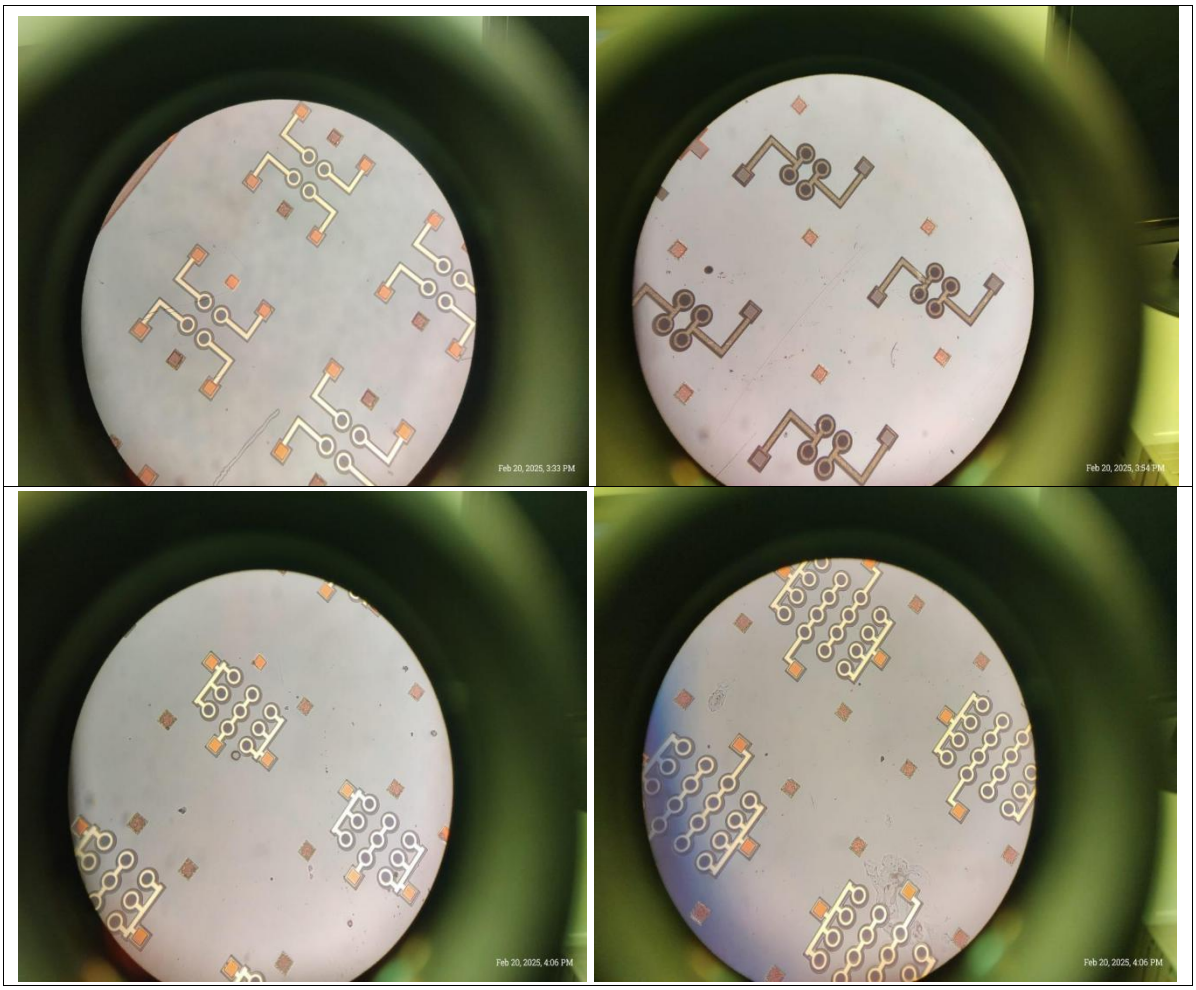

Figure 34:Microscope image after Lithography.

4.3.9.2 SiO_2 Deposition Using PECVD

Step 1. Wafer Preparation:

It was dried using nitrogen gas.

Step 2. PECVD System Setup:

The cleaned wafer was loaded into the PECVD chamber.

Step 3. Deposition Parameters Setup:

The RF power was set to 1000 W to generate plasma.

The chamber temperature was maintained at 70°C for optimal deposition.

The gas flow rates were adjusted as follows:

N_2O: 40 sccm

SiH_4: 16 sccm

The deposition rate was set to 500 Å/min.

Step 4. SiO_2 Deposition Process:

The plasma was started to initiate the chemical reaction between silane (SiH_4) and nitrous oxide (N_2O).

The deposition was allowed to continue for 2 minutes, ensuring a uniform 150 nm SiO_2 layer.

4.3.9.3 N and P Pad Contact Liftoff

Objective: To remove excess metal and photoresist after PECVD.

Step 1: Soaking & Photoresist Removal

Lift-Off Resist (LOR) Removal:

The wafer was immersed in a boilled PG remover for 35 mins to break down the LOR layer.

Step 2: Sequential Cleaning

Q-tip Cleaning:

The wafer was gently scrubbed with a Q-tip dipped in acetone.

Boiling Acetone:

The wafer was immersed in boiling acetone (200°C) for 10 minutes.

IPA Bath:

The wafer was then transferred to isopropyl alcohol (IPA).

Final Drying:

The wafer was dried using N_2 gas to prevent contamination.

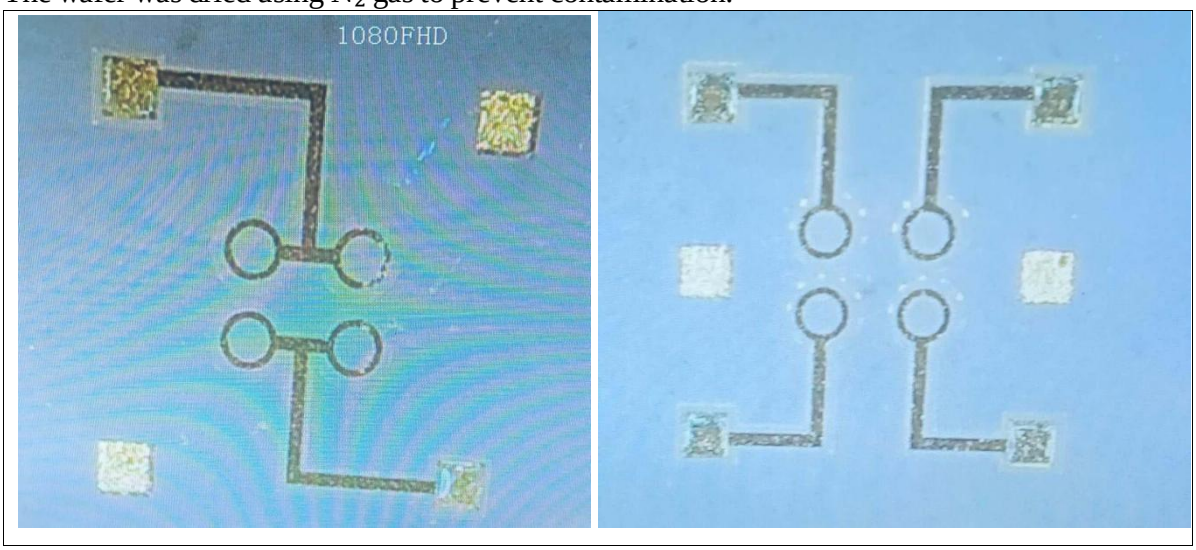

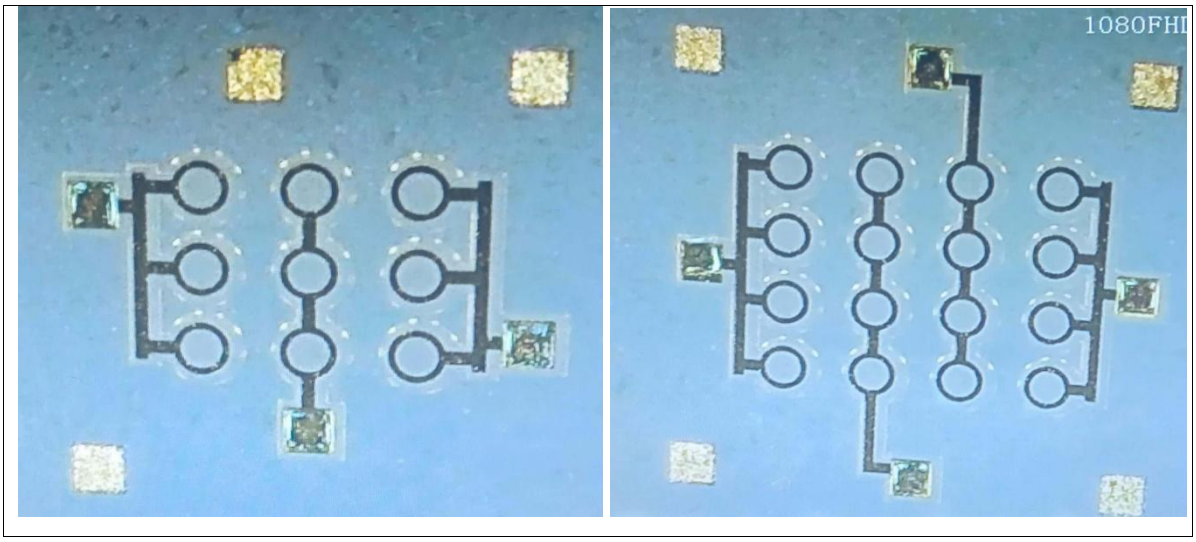

Figure 35:Microscope image of Final devices

4.3.10 Dicing for separation of each Design.

4.3.10.1 Mounting the Wafer:

A glass wafer was placed on a heater, and wax was applied. As the wax corroded, a sapphire wafer was mounted on it.The glass wafer was secured to a dicing tape, which was mounted on a dicing frame.

The tape was properly stretched to avoid wrinkles.

The wafer center was aligned with the frame's center for uniform stability.

The adhesive side of the tape securely held the wafer while allowing easy removal post-dicing.

4.3.10.2 Setup and Inspection:

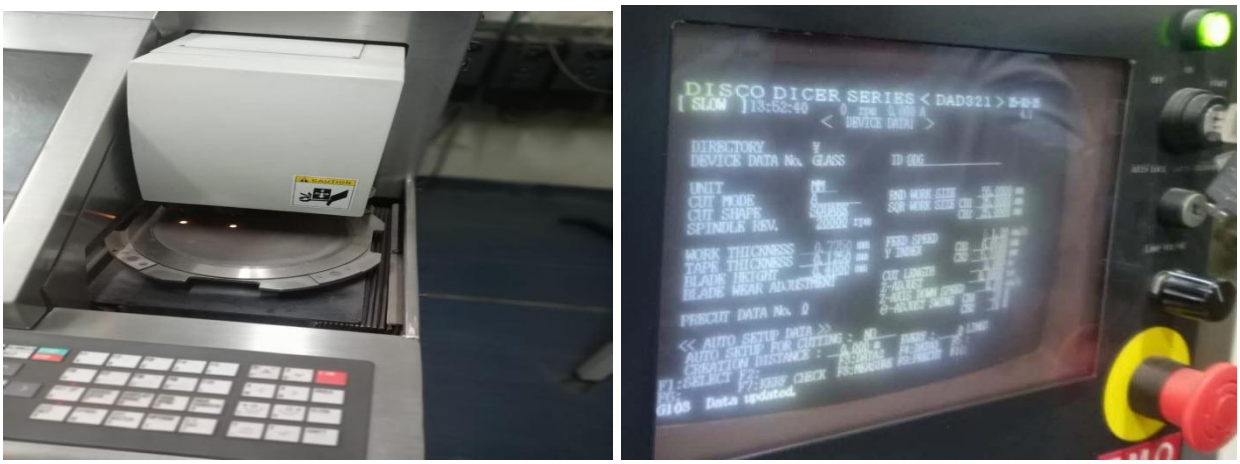

Figure 36:Dicing setup

The wafer was inspected under a microscope to identify alignment markers and dicing lines.

Manual alignment was performed to set the dicing lines accurately.

4.3.10.3 Blade Selection:

An appropriate diamond dicing blade was chosen based on:

Material: Sapphire.

Work Thickness: 775 µm.

Tape Thickness: 125 µm.

Blade height: 400 µm.

4.3.10.4 Cooling System:

The cooling water system was ensured to be operational to prevent overheating during dicing.

4.3.10.5 Parameters Setup:

Blade rotation speed was set to 20,000 RPM.

Feed rate was set to 1 mm/sec.

Cut depth was set to 500 µm.

Cooling water flow was set to 1 liter/minute.

4.3.10.6 Dicing Process

4.3.10.6.1 Alignment:

The wafer's scribe lines were aligned with the blade using the Disco machine's manual controls.

4.3.10.6.2 Full Wafer Dicing:

The dicing process was initiated:

The machine moved the wafer along the pre-set lines while the blade rotated.

The process was monitored for vibrations or misalignment during cutting.

4.3.10.6.3 Coolant Monitoring:

The cooling water was continuously sprayed on the blade and wafer to reduce heat and prevent chipping.

Figure 37:Final dicing wafer view.

5

RESULTS

5 RESULTS AND DISCUSSION

5.1 Band diagram

For the structure made in sentaurus, a band diagram is simulated at a reverse bias of -4V and the superlattice part is shown in it.

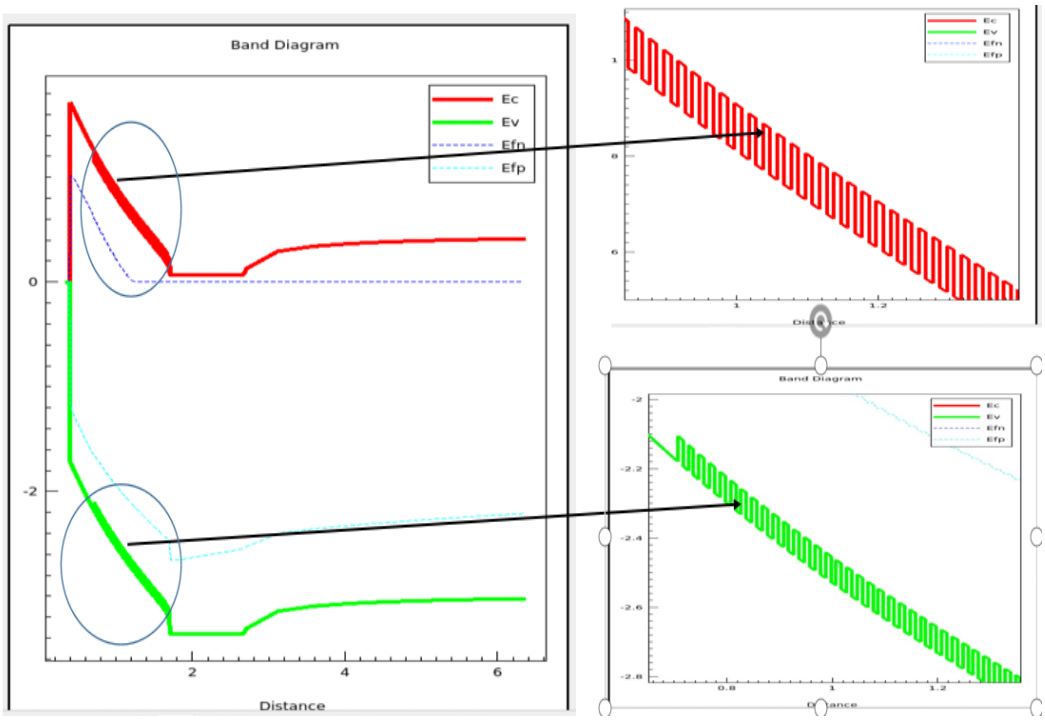

Figure 38:Final dicing wafer view.

The fig.5.4 is the band diagram for the GaN/InGaN superlattice part of 50 periods with 1nm each. The Indium composition in InGaN is 4% i.e., the bandgap of $In_{0.04}Ga_{0.96}N$ according to the Vegard's law is 3.26eV.

5.2 ITO transmittance

For the ITO-coated glass plate with a thickness of 100 nm, the transmittance was evaluated across a wavelength range of 200 nm to 800 nm. At 380 nm, the transmittance was recorded to be 86.13%.

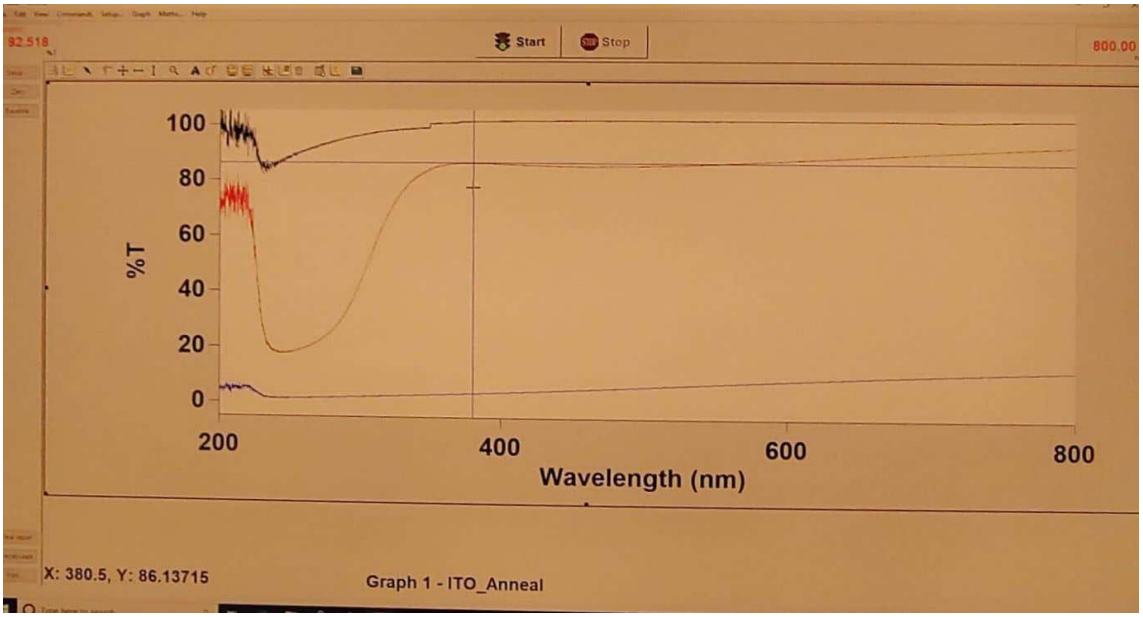

Figure 39:Transmittance of ITO vs wavelength

5.3 Optical Properties vs Wavelength:

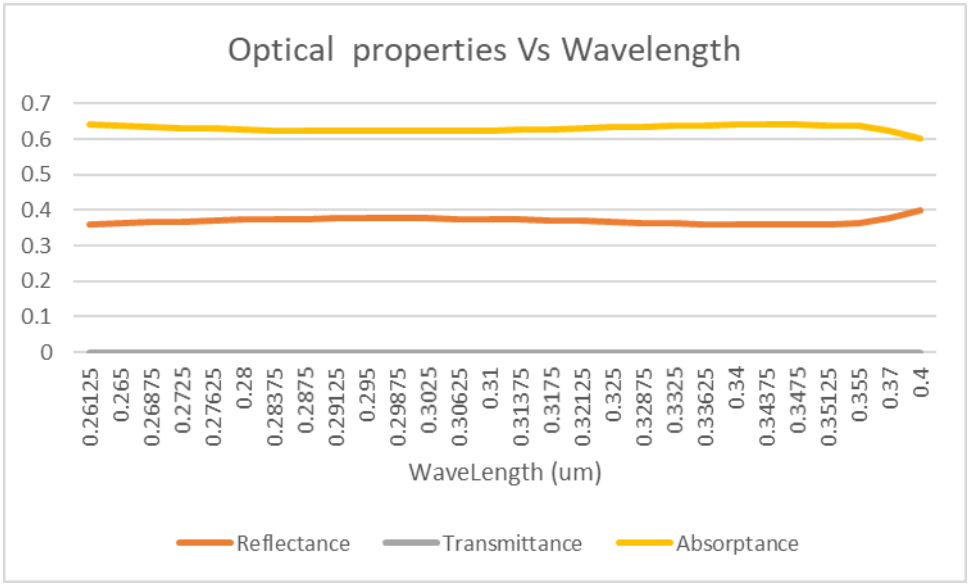

Figure 40:Optical properties (%) vs Wavelength(nm)

1. Absorption (Blue Line):

The absorption is very high (~6 to 6.5) across the 250–400 nm wavelength range. Slight decrease in absorption is observed as the wavelength increases beyond 400 nm, indicating a strong UV sensitivity that tapers near the visible range. This suggests that the material is highly effective at absorbing UV light, particularly in the near UV range (350–400 nm).

2. Reflection (Yellow Line):

The reflection remains very low, generally below 40%, throughout the wavelength range. Slight rise in reflection is seen beyond 400 nm, but it still remains minimal. This means very little light is lost to surface reflection, which is ideal for enhancing the efficiency of photodetectors.

3. Transmittance (Green Line):

Transmittance is nearly zero, which confirms that most incident light is absorbed, not passed through. This is expected and desirable in a UVabsorbing photodetector material, as it indicates maximal photon capture.

Table 4:Optical properties(%) vs Wavelength(nm)

wavelength (um)	Reflectance	Transmittance	Absorptance
0.25	0.336	0	0.664
0.25375	0.3472	0	0.6528
0.2575	0.2551	0	0.6449
0.26125	0.3596	0	0.6404
0.265	0.3628	0	0.6372
0.26875	0.3662	0	0.6338
0.2725	0.3687	0	0.6313
0.27625	0.371	0	0.629
0.28	0.3738	0	0.6262
0.28375	0.3753	0	0.6247
0.2875	0.3758	0	0.6242
0.29125	0.377	0	0.623
0.295	0.3782	0	0.6218
0.29875	0.3778	0	0.6222
0.3025	0.3768	0	0.6232
0.30625	0.3758	0	0.6242
0.31	0.3748	0	0.6252
0.31375	0.3734	0	0.6266
0.3175	0.3714	0	0.6286
0.32125	0.3688	0	0.6312
0.325	0.3661	0	0.6339
0.32875	0.364	0	0.636
0.3325	0.3624	0	0.6376
0.33625	0.3612	0	0.6388
0.34	0.3601	0	0.6399
0.34375	0.3595	0	0.6405
0.3475	0.3597	0	0.6403
0.35125	0.3607	0	0.6393
0.355	0.3619	0	0.6381
0.37	0.3769	0	0.6231
0.4	0.398	0	0.602

5.4 Fabricated device IV characteristics in dark

The IV characteristics of the fabricated UV photodetector is plotted using Ecopia LED chip tester

in dark conditions and also to check reverse breakdown voltage.

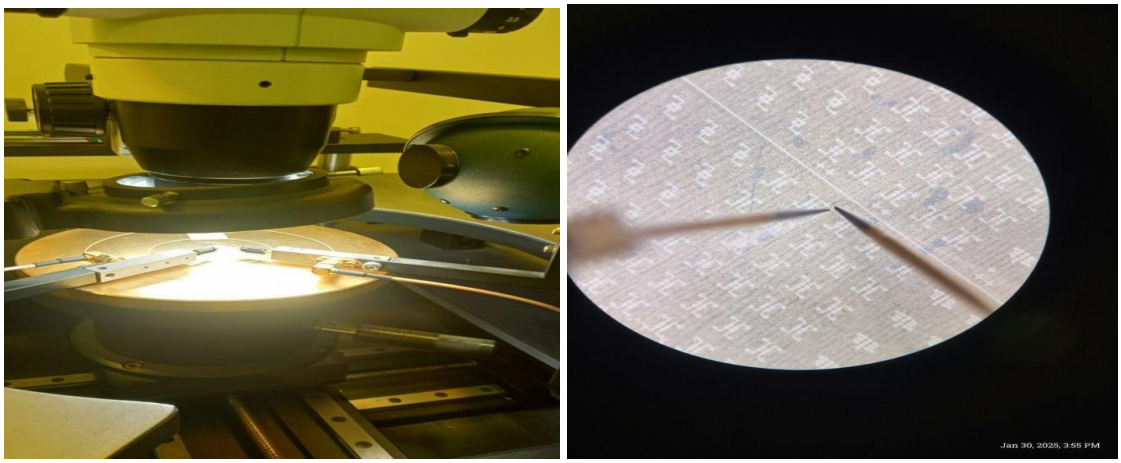

Figure 41:Probes are in contact with the n and p pad contacts

To check breakdown voltage, when a reverse bias voltage of -2V to 10V is applied to the fabricated device, I-V characteristics are observed as follows in with incident light and the reverse breakdown voltage is around 1.45 V.

Table 5:Cut in voltages with respective different arrays

Design	**Configuration**	**Cut in Voltage**
1st Design	2×2 Series Array	1.25 V
2nd Design	2×2 Parallel	1.45 V
3rd Design	3×3 Array	2.6 V
4th Design	4×4 Array	5.54 V

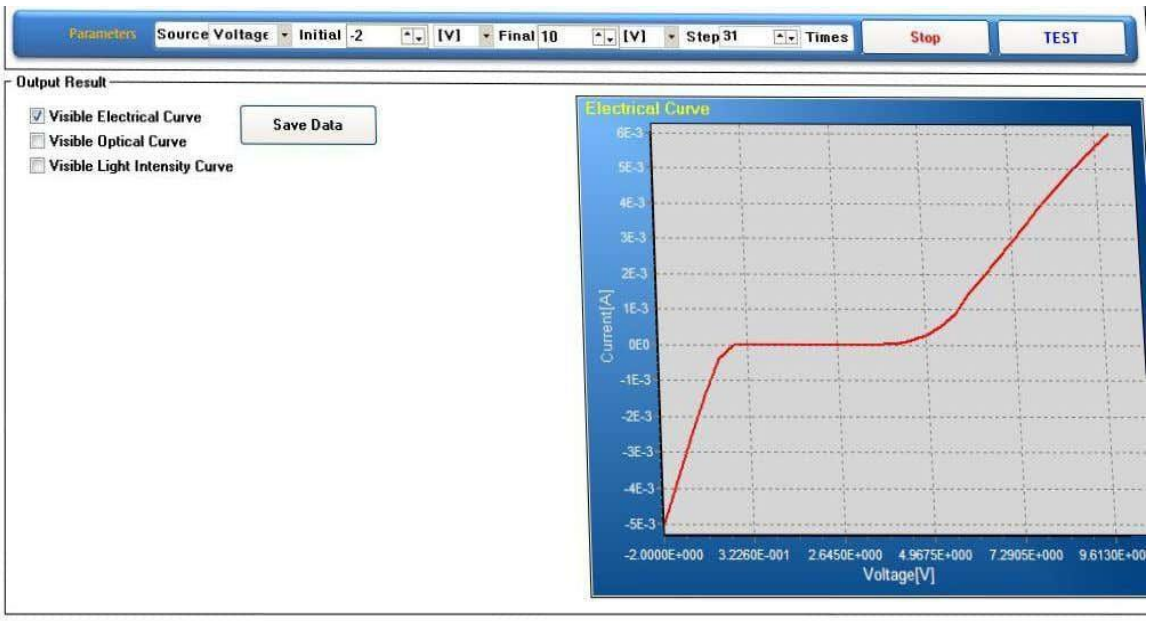

Figure 42:I-V characteristics of the photodetector in absence of light (-2 to 10V)

5.5 Simulation results

contact	voltage	electron current	hole current	conduction current
n-contact	0.000E+00	7.727E-13	0.000E+00	7.727E-13
p-contact	-3.000E+00	-1.922E-13	0.000E+00	-1.922E-13

Reflectance, Transmittance and Absorptance

	TE	TM	mean
R:	0.3907	0.3907	0.3907
T:	0.0000	0.0000	0.0000
A:	0.6093	0.6093	0.6093

conduction current
-6.979E+12
-1.889E-10

Table 6:2-D Simulation result

Parameter	Value
Wavelength (λ)	381 nm
Incident Light Power	1×10^{-6} W/cm²
Light Current	-1.88×10^{-10} A
Dark Current	-1.922×10^{-13} A
Photocurrent (Iph)	1.86×10^{-10} A
Responsivity (R)	0.186 A/W
External Quantum Efficiency (EQE)	61.0 %
Detectivity (D*)	~3.75×10^{10} Jones
Absorption	60.93 %
Reflectance	39.07 %

6

CONCLUSION AND FUTURE SCOPE

6 CONCLUSION AND FUTURE WORK

6.1 Conclusion

The proposed PIN-based photodetector array has been designed and simulated using Synopsys Sentaurus TCAD to validate its electrical and optical characteristics. Following the simulation, the fabrication of the UV photodetector array was successfully completed. This device is intended to deliver enhanced performance under low-light conditions, making it suitable for a variety of applications across multiple fields.The improved features of the developed photodetector include high responsivity and low noise, resulting in a superior signal-to-noise ratio (SNR) within the 350–450 nm wavelength range, targeting the UV-Blue spectral region. Upon characterization, the device is expected to demonstrate performance metrics that surpass those of comparable photodetectors currently available in the market.

6.2 Future work

Now the fabricated device can be packaged and characterized for the photoelectric performance. Once proved and successfully validated, the product can be made available for the industry to be commercialized and can be used for the biomedical applications, space applications and optoelectronic devices etc.

7 REFERENCES

[1] N. D. Gupta, K. Sumanth, P. Yashwanth, K. Raghunath, A. Kumar, K. Singh, and M. Mathew, "Design and Fabrication of a Photodetector for UV/Blue Wavelength Region for Low-Light Intensity Levels Using InGaN/GaN Superlattice Structure," IEEE Transactions on Electron Devices, vol. 71, no. 9, pp. 5494–5502, Sept. 2024. doi: 10.1109/TED.2024.3427094.

[2] Z. Lv, Z. Liao and H. Jiang, "InGaN/GaN Visible-Light Heterojunction Phototransistor Featuring High Responsivity, High Speed, and Bias-Controlled Wavelength-Selectivity," IEEE Electron Device Letters, vol. 42, no. 9, pp. 1362–1365, Sept. 2021. doi: 10.1109/LED.2021.3097048

[3] G. Wang, H. Lu, D. Chen, F. Ren, R. Zhang, and Y. Zheng, "High Quantum Efficiency GaN-Based p-i-n Ultraviolet Photodetectors Prepared on Patterned Sapphire Substrates," IEEE Photonics Technology Letters, vol. 25, no. 7, pp. 652–654, Apr. 2013. doi: 10.1109/LPT.2013.2248056.

[4] M. Elbar, A. M. A. Amin, and A. M. A. El-Badry, "Design and Simulation of InGaN/GaN p-i-n Photodiodes," Physica Status Solidi (a), vol. 215, no. 9, p. 1700803, May 2018. doi: 10.1002/pssa.201700803.

[5] M. Monavarian and A. A. Balandin, "Analysis of External Quantum Efficiencies of GaN Homojunction p-i-n Ultraviolet Photodetectors," IEEE Journal of the Electron Devices Society, vol. 9, pp. 236–242, Mar. 2021. doi: 10.1109/JEDS.2021.3059460.

[6] M. D. Mathew, R. Jha, and M. G. Krishna, "Effect of Indium Composition on the Microstructural Properties and Performance of InGaN/GaN MQWs Solar Cells," IEEE Transactions on Electron Devices, vol. 67, no. 3, pp. 944–951, Mar. 2020. doi: 10.1109/TED.2020.2966330.

[7] Ting Li, J. C. Carrano, J. C. Cambell, M. Schurman and I. Ferguson, "Analysis of external quantum efficiencies of GaN homojunction p-i-n ultraviolet photodetectors," in IEEE Journal of Quantum Electronics, vol. 35, no. 8, pp. 1203-1206, Aug. 1999, doi: 10.1109/3.777221

[8] J. Pereiro et al., "Optimization of InGaN–GaN MQW Photodetector Structures for High-Responsivity Performance," in IEEE Journal of Quantum Electronics, vol. 45, no. 6, pp. 617-622, June 2009, doi: 10.1109/JQE.2009.2013140.

[9] N. Gupta, V. Janyani, M. Mathew, M. Maun and R. Singh, "Design and Fabrication of

InGaN/GaN Superlattice based Solar Cell using Photonic Crystal Structure at the Front Surface," Journal of Nanophotonics, vol. 12, no. 4, p. 043505, 2018
[10] F. Zetong, "An Analysis of GaN-based Ultraviolet Photodetector," IOP Conf. Series: Materials Science and Engineering, vol. 738, p. 012006, 2020

[11] KnowElectronic, "What is PIN Diode? - Structure, Working, Characteristics & Its Applications," [Online]. Available: https://www.knowelectronic.com/pin-diode/.
[12] K.M. Kelchner, S.P. DenBaars, J.S. Speck, Chapter 4 – "GaN Laser Diodes on Nonpolar and Semipolar Planes", Semiconductors and Semimetals, Volume 86, Pages 149-182, 2012
[13] R. Pant, D. K. Singh, A. M. Chowdhury, B. Roul, K. K. Nanda and S. B. Krupanidhi, "Next-generation self-powered and ultrafast photodetectors based on III- nitride hybrid structures," APL Materials, vol. 8, p. 020907, 2020
[14] H.S. Shan, X.Y. Li, B. Chen, S.F. Ma, L. Li and B.S. Xu, "Effect of Indium Composition on the Microstructural Properties and Performance of InGaN/GaN MQWs Solar Cells," IEEE Access, vol. 7, pp. 182573-182579, 2019.
[15] Pernot, Cyril & Hirano, Akira & Iwaya, Motoaki & Detchprohm, Theeradetch & Amano, H. & Akasaki, Isamu, "Low-Intensity Ultraviolet Photodetectors Based on AlGaN", Japanese Journal of Applied Physics, 1999
[16] Padma, G. S., Singh, S., Mathew, M., Singh, K., Joshi, B. C., Das, S., & Dhanavantri, C, "Fabrication of GaN/InGaN MQW blue light emitting diode", In Journal of Optics, 2012 (Vol. 41, Issue 4, pp. 198–200). Springer Science and Business Media LLC. https://doi.org/10.1007/s12596-012-0083-z
[17] P. -C. Chang, C. L. Yu, S. J. Chang, K. H. Lee, C. H. Liu and S. L. Wu, "High-Detectivity Nitride-Based MSM Photodetectors on InGaN–GaN Multiquantum Well With the Unactivated Mg-Doped GaN Layer," in IEEE Journal of Quantum Electronics, vol. 43, no. 11, pp. 1060-1064, Nov. 2007, doi: 10.1109/JQE.2007.907249.
[18] J. Kang, M. Li, Q. Li, W. Wang, F. Chen and J. Zhang, "Optimal design of superlattice periods and well doping for III-nitride intersubband photodetectors," 2017 International Conference on Numerical Simulation of Optoelectronic Devices (NUSOD), Copenhagen, Denmark, 2017, pp. 215-216, doi: 10.1109/NUSOD.2017.8010068.
[19] A. V. Lobanova, A. L. Kolesnikova, A. E. Romanov, S. Y. Karpov, M. E. Rudinsky and E. V. Yakovlev, "Mechanism of stress relaxation in (0001) InGaN/GaN via formation

of V-shaped dislocation half-loops," Appl. Phys. Lett., vol. 103, no. 15, p. 152106, 2013
[20] Daniel Nilsson, Chapter-4, “Doping of high-Al-content AlGaN grown by MOCVD”, Linkoping Studies in Science and Technology, Dissertation No. 1597, Pages: 19–26, 2014
[21] X. Zheng, R. Horng, D. S. Wuu, M. Chu, W. Liao, M. Wu, R. Lin and Y. Lu, "High quality InGaN/GaN heterojunctions and their photovoltaic effects," Applied Physics Letters, vol. 93, p. 261108, December 2008
[22] Hu, Wei & Yang, Jinlong, “Two-dimensional van der Waals heterojunctions for functional materials and devices”, Journal of Materials Chemistry C. 5. 10.1039/C7TC04697A, 2017
[23] Donald A. Neamen, Chapter 14 - “Semiconductor Physics and Devices”, Fourth edition, Page 640, 2012
[24] Tu, Ru-Chin & Tun, C. & Sheu, Jinn-Kong & Kuo, Wei-Hong & Wang, Te-Chung & Tsai, Ching-En & Hsu, Jungtsung & Chi, Jim & Chi, Gou-Chung, “Improvement of InGaN/GaN laser diodes by using a Si-doped In0.23Ga0.77N/GaN short-period superlattice tunneling contact layer”, Electron Device Letters, IEEE, 2003. 24. 206 - 208. 10.1109/LED.2003.810889.